
**STUDY OF ELECTRICAL TRANSPORT PROPERTIES
OF CONDUCTING POLYMER PEDOT:PSS IN
CONFINED CHANNELS**

A Thesis

*Submitted in partial fulfillment for the degree
of*

MASTER OF SCIENCE

(Materials Science)

by

Sukanya Das



Chemistry and Physics of Materials Unit
JAWAHARLAL NEHRU CENTRE FOR ADVANCED SCIENTIFIC RESEARCH
(Deemed University)
Bangalore – 560064, India
April 2018

Dedicated to my family

DECLARATION

I hereby declare that the matter embodied in the thesis entitled “**Study of Electrical Properties of Conducting Polymer PEDOT:PSS in Confined Channels** ” is the result of investigations carried out by me at the Chemistry and Physics of Materials Unit, Jawaharlal Nehru Centre for Advanced Scientific Research, Bangalore, India under the supervision of Prof. K. S. Narayan and that it has not been submitted elsewhere for the award of any degree or diploma.

In keeping with the general practice in reporting scientific observations, due acknowledgement has been made whenever the work described is based on the findings of other investigators.

SUKANYA DAS

JAWAHARLAL NEHRU CENTRE FOR ADVANCED SCIENTIFIC RESEARCH
JAKKUR, BANGALORE, 560064. INDIA

K.S. NARAYAN

Professor and Dean (R&D)

Phone: 080-2208-2822

FAX: 91 80 22082766

E-mail: narayan@jncasr.ac.in



CERTIFICATE

2nd April, 2018

I hereby certify that the matter embodied in this thesis entitled “*Electrical Transport Properties of conducting polymer PEDOT:PSS in confined channels*” has been carried out by Ms. Sukanya Das at the Chemistry and Physics of Materials Unit, Jawaharlal Nehru Centre for Advanced Scientific Research, Bangalore, India under my supervision and that it has not been submitted elsewhere for the award of any degree or diploma.

Prof.K.S. Narayan
(Research Supervisor)

Acknowledgements

I would like to thank my research supervisor Prof. K.S. Narayan for his guidance, motivation and encouragement that he has provided throughout the period of my M.S work. His valuable instructions, suggestions and comments have helped me immensely in preparing the thesis work. His hardworking nature, enthusiasm for science and ability to create interests among students to investigate a research problem have inspired me truly.

I thank Prof. C.N.R Rao for being a constant source of inspiration.

I would like to sincerely thank past and present chairman and also Integrated Ph.D coordinator of Chemistry and Physics of Materials Unit, Prof. S. Balasubramanian and Prof. Chandrabhas Narayan for their invaluable support. I thank all the professors under whom I have taken M.S. course works, starting from Prof. S. Balasubramanian, Prof. Umesh Waghmare, Prof. Shobhana Narasimhan, Prof. N. Chandrabhas, Prof. K.S. Narayan, Prof. Rajesh Ganapathy, Prof. Meher K. Prakash and Prof N. S. Vidhyadhiraja for valuable discussions and teaching throughout the coursework.

I am thankful to my past and present labmembers, Dr. Ravichandran Shivanna, Dr. Suman Banerjee, Dr. Prashant Kumar, Ashar, Swathi, Raaghesh, Apoorva, Ganesh, Deepak, Anaranya, Sumukh, Anil Kumar and Azeez for their valuable discussions, insights and cooperation which have always helped me working in lab. Ofcourse I

have learned many things from the group meetings held in our lab where each and everyone's comments and suggestions have helped me figure out problems.

I extend my gratitude to all staff members in Library, Academic and Administration sections. And ofcourse mess staffs for their level best to cook different types of food and keep us happy and working in our research life.

I sincerely acknowledge all my friends from Integrated Ph.D 2015 batch- Rajendra, Narendra, Niloyendu, Janaky and Lakshay. They have been constantly been standing beside me in anytime of need and have been helped rejoice JNC campus life.

I thank my family, my parents and my sister for their love and encouragement and for whom I have been in JNCASR today to study and further carry on in my research life.

Finally, I am happy to be a part of JNCASR. The surroundings, working environment, cleanliness, and obviously the beautiful plants and flowers blooming due to the hardwork of JNC gardeners are worth mentioning that have added to a healthy and wonderful life in campus.

JNCASR,
BANGALORE
April 2018

Sukanya Das

Preface

In this thesis, the electrical transport properties of conducting polymer PEDOT:PSS due to confinement effects are studied. It is shown that the change in carrier transport in PEDOT:PSS is effected below a certain characteristic length scale.

Chapter 1 introduces briefly to mixed ionic-electronic conducting polymers and the difficulty to probe the simultaneous ionic and electronic carriers in these mixed conducting systems. This thesis describes how confinement of polymers may lead to morphology change of conducting polymer blends below a characteristics confinement length scale that can be related to the change in transport mechanisms of the polymer blend.

Chapter 2 deals with Materials and Methods used in the experiment. Conducting polymer PEDOT:PSS, porous membrane as AAO are some of the prime materials used. Impedance measurements (at varying temperature) using parameter analyzer, lock-in amplifier and some AFM and CAFM studies to probe the measurements at nanoscale are discussed.

The results and discussions are described in details in Chapter 3. The a.c conductivity and low-temperature studies help in deciding the transport taking place in bulk and on confinement. The optimization steps required, some calculations needed to take into account the affecting factors are briefly discussed.

Chapter 4 describes the summary of the thesis work, some further improvements and simulations required to support the work. This work further can be extended to study ion transport dynamics in confined vertical channels. Simultaneous study of moving front of ions dynamics in confined channels with the changing morphology of medium of transport, i.e., the conducting polymer blend can be studied. The thesis opens up template-structure transport studies for conducting polymers.

TABLE OF CONTENTS

| | |
|--|-----------------|
| <i>Chapter 1: Introduction</i> | <i>...1</i> |
| <i>1.1 Conducting Polymers</i> | <i>...2-4</i> |
| <i>1.2 Electronic properties of conducting polymers</i> | <i>...4-6</i> |
| <i>1.3 Mixed Ionic-Electronic Conducting Polymers</i> | <i>...6-7</i> |
| <i>1.4 PEDOT:PSS</i> | <i>...7</i> |
| <i>1.4.1 Structure, morphology and conduction in PEDOT:PSS</i> | <i>...7-8</i> |
| <i>1.4.2 Hopping transport in PEDOT:PSS</i> | <i>...9-10</i> |
| <i>1.4.3 Mesoscopic 2D transport in PEDOT:PSS</i> | <i>...10-12</i> |
| <i>1.5 Polymers in confinement</i> | <i>...12</i> |
| <i>1.5.1 Brief definitions from statistical point of view</i> | <i>...12-14</i> |
| <i>1.5.2 Polymer dynamics in confinement</i> | <i>...14-15</i> |
| <i>1.6 Overview of thesis</i> | <i>...15-16</i> |
| <i>References</i> | <i>...16-21</i> |

Chapter 2: Materials and Methods

| | |
|--|-----------------|
| <i>2.1 Materials</i> | <i>...22</i> |
| <i>2.1.1 PEDOT:PSS</i> | <i>...22-23</i> |
| <i>2.1.2 Ultrathin AAO membranes</i> | <i>...23-24</i> |
| <i>2.1.3 Additive(DMSO)</i> | <i>...24-25</i> |
| <i>2.2 Device Fabrication and characterization</i> | <i>...25-27</i> |
| <i>2.3 Instruments and sample characterization</i> | |
| <i>(1) AFM (Atomic Force Microscopy)</i> | <i>...28-30</i> |
| <i>(2) CAFM (Conductive Atomic Force Microscopy)</i> | <i>...31-32</i> |

| | |
|----------------------------------|----------|
| (3) Impedance Spectroscopy | ...32-34 |
| (4) Low-temperature measurements | ...34 |
| References | ...35 |

Chapter 3: Results and Discussions

3.1 Measurements in bulk PEDOT:PSS

3.1.1 D.C conductivity

| | |
|---------------------------------|----------|
| (1) Pristine PEDOT:PSS (Al4083) | ...36-39 |
| (2) Pristine PEDOT:PSS (PH1000) | ...39-41 |
| (3) PEDOT:PSS+Co-solvents | ...41-43 |

3.1.2 Temperature dependent d.c conductivity of PEDOT:PSS

...44

3.1.3 A.C Conductivity

...45-47

3.2 Measurements in confinement

3.2.1 dc conductivity (macroscopic measurements)

... 48-51

3.2.2 dc conductivity using CAFM

...51

(1) Pristine PEDOT:PSS in 20nm pores

...52-53

(2) Pristine PEDOT:PSS in 50nm pores

...54-55

(3) Pristine PEDOT:PSS in 100nm pores

...56-59

3.2.3 Temperature dependent a.c conductivity

...59-62

3.3 Schematic of polymer morphology in confinements

...63

References

...64-65

Chapter 4

Summary and outlook ...66-67

References68

CHAPTER 1

INTRODUCTION

Electrical transport in conducting polymers are fundamentally different from the conventional metals. Doping of conducting polymers involve introduction of ionic species which causes disorder. In the context of electrical properties, disorder influences charge carrier transport. Disorder induced electrical transport is described in terms of quasi-particles such as solitons, polarons and bi-polarons whose effective masses are greater than electron masses. Electronic transport thus happens in the background of ionic displacement. This picture roughly describes the mixed electronic-ionic conduction state in conducting polymers. Simultaneous probing of electronic and ionic carrier conduction in these mixed conducting polymers is difficult due to the coupling of the charge carriers and variation of film morphology due to the perturbations induced in the system during the carrier transport.

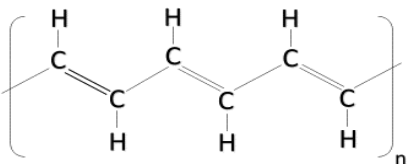
Conformation of polymers in confinement plays a major role in aspect of morphology and transport mechanism of polymers. In this thesis, attempt has been made to qualitatively control the ionic and electronic conduction on the grounds of polymer conformation in confined channels. It is shown that PEDOT:PSS, a conducting polymer blend possessing both ionic and electronic carriers when confined in cylindrical channels is restricted from some degree of freedom in particular direction while transport enhances along other direction. Changing morphology of the polymer blend is reflected from changing length scales of confinement. This helps to find the dominating carrier conduction beyond a characteristic confinement length scale.

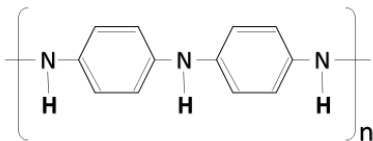
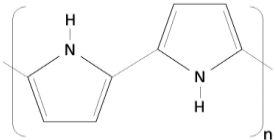
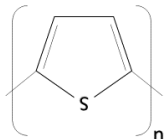
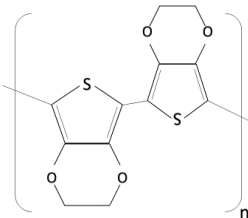
1.1 Conducting polymers:

Conducting Polymers (CP) remarkably led the transition from the era of ‘plastic’ insulators (polymers) to nearly metallic polymers. Conducting polymers are often called ‘synthetic metals’. Easy processability, flexibility, shaping polymers into complex multi-layer/polymer designs, light weight are some of the properties that led scientists and industrialists to find their novel applications. CPs have interesting characteristics of combined electronic properties of semiconductors and metals and mechanical properties of polymers.

The pioneers of Conducting Polymers in 1976 are Alan MacDiarmid, Hideki Shirakawa and Alan J. Heeger who founded the enhancement of conductivity of the polymer, polyacetylene by seven orders of magnitude after doping with iodine. This great work led them to earn the Nobel Prize in Chemistry in 2000 [1,2,3]. This discovery followed synthesis of many more conducting polymers such as Polypyrrole (PPY), Polyaniline (PANI), Poly(phenylene)s (PPs), Poly(p-phenylene) (PPP), poly(p-phenylenevinylene) (PPV), poly(3,4-ethylene dioxythiophene) (PEDOT), polyfuran (PF) and other polythiophene (PTh) derivatives. These polymers have interesting electrical characteristics, reversible doping-dedoping procedure, simple processability and controllable electrochemical properties.

Some conducting polymers with their structure and conductivities are given below [4]:

| CONDUCTING POLYMER (Year of discovery) | STRUCTURE | CONDUCTIVITY (S/m) |
|---|---|--------------------|
| Polyacetylene (1977) |  | $10^1 - 10^3$ |

| CONDUCTING POLYMER (Year of discovery) | STRUCTURE | CONDUCTIVITY (S/cm) |
|---|---|---------------------|
| Polyaniline (1980) |  | 0.30 – 2.00 |
| Polypyrrole (1979) |  | 1 – 10 |
| Polythiophene (1981) |  | 0.10 – 10 |
| Poly(3,4-ethylene-dioxythiophene) (1980) |  | 3.00 |

Organic electronic materials have found application in many fields. In the undoped semiconductor state they are used as an active layer in organic solar cells, LEDs. The first organic light emitting diode (OLED) was fabricated in 1990s. This led to the vast opening in the field of Organic Electronics [5,6]. Organic photovoltaics (OPVs) and thin film transistors (OTFT) became a wide field of interest for scientists. Researches on OLED, OTFT and OPVs were carried out extensively. Optimization of OPVs led a new trend of optimizing organic electronics with biology [7, 8]. Due to soft nature and flexibility, CPs act as ideal materials for interfacing with biological cells and tissues. Berggren and Richter-Dahlfors describes the

coupling of organic electronic (and optoelectronic) devices with biological objects. In the doped state CPs are used as transparent electrodes, biosensors [9,10], electrically stimulated cell growth on conducting polymers surfaces [11, 12].

1.2 Electronic properties of conducting polymers

A general characteristic of conducting polymers is the presence of double bonds alternating with single bonds along the polymer chain, i.e. conjugated bonds. Electron configuration of the six electrons in a carbon atom (in its ground state) is $1s^2 2s^2 2p^2$. The electrons in the core orbitals do not contribute to the chemical bonding. The s and p orbitals combine to form hybrid orbitals which give rise to triple, double, or single bonds.

The electrons in the π -bonds are weakly bound and so are easily delocalized. These delocalized π electrons are the reason for conduction in these materials. In conjugated conducting polymers, sp^2 hybridization is necessary for conduction (Figure 1.2). Assuming that single and double bonds have same bond length, Bloch's theory tells atoms with half-filled shells have partially filled bands with metallic properties.

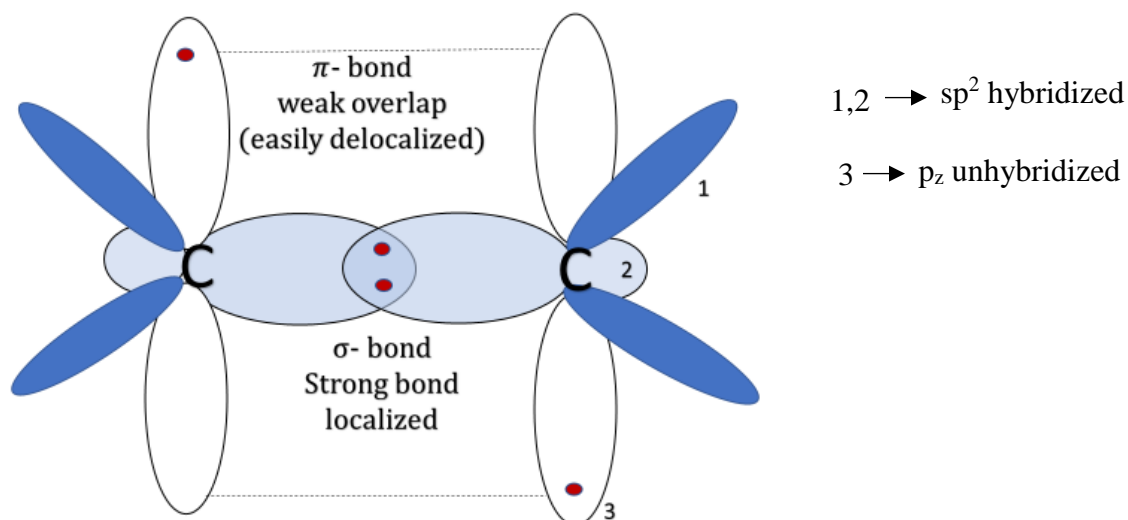


Figure 1.2: Bonding in conducting conjugated polymers.

But the assumption that double and single bonds are identical is an ideal condition. Actually, the single and double bond lengths are non-identical (single bonds being longer than double bonds) which gives rise to Peierls instability [13] that splits the continuous band into two sub-bands- a completely filled valence band (highest occupied molecular orbital, HOMO level) and an empty conduction band (lowest unoccupied molecular orbital, LUMO level), separated by an energy gap. Hence, the material behaves like a semiconductor.

The conductivity of polymer, σ , is proportional to carrier concentration, n , and the carrier mobility, μ , i. e.

$$\sigma = e n \mu \quad \dots (1)$$

For intrinsic conductivity, n decreases exponentially with increasing band gap, since the conjugated polymers have relatively large band gap, consequently, n is low at normal temperature. A low value of 'n' leads to a low value of conductivity of undoped polymers even-though the polymers have high carrier mobility [14]. The conductivity strongly depends on the temperature. For metals, it decreases with increasing temperature, whereas for semiconductors like conducting polymers it increases.

Doping: Through the process of doping, conductivity can be increased in conjugated polymers. When an electron is removed from the valence band by oxidation (p-doping) or added to the conduction band by reduction (n-doping) the polymer become highly conductive. Doping creates defects (polaron, bipolaron and soliton) that can travel through the backbone of the polymer.

The doping process produce number of carriers in polymer, but these carriers should be mobile in order to add to conductivity, eq. [1]. Doping creates new electronic states in the band gap of material. At high doping concentrations these states interact strongly with each other, and as a result, the overlap of their electronic wave functions forms a continuum band of electronic state within the band gap instead of discrete levels. The mechanism of carrier

transport in conducting polymer is like hopping transport as in amorphous semiconductors than band transport (as in crystalline semiconductors). Thus, doping creates an active sites (polarons) which enable the carriers (electronic & holes) to hop from one site to another. This is how conductivity increases by doping in conducting polymers.

1.3 Mixed Ionic-Electronic Conducting polymers

Mixed ionic-electronic conductors (MIECs) are materials that conduct both electronic (electrons or holes) and ionic charge carriers [15]. Certain organic semiconductors are MIECs; the ability to transport ionic and electronic charge finds use in organic electronics in a wide range of promising applications including gas sensors [16,17], light-emitting electrochemical cells [18, 19], superconductors [20,21], and transistors [22,23]. MIECs based on organic semiconductors are used in biosensors to detect the presence of ions in biological tissue [24]. An example of biosensor device is the organic electrochemical transistor [25] (OECT). The applied voltage injects ions from the electrolyte into the polymer film. The ions displace electronic charge carriers that evacuate the thin film across the source electrode, that results in the conversion of an ionic current to an electrical signal. The role of ionic carriers in electronic carrier transport is slightly complex to understand. Accurate measurement of the mobility of ionic species in an organic MIEC is important in characterizing ion transport. But mobility is challenging to determine because standard techniques to measure charge carrier mobility, such as time of flight measurements [26], are difficult to implement in organic MIECs.

Stavriniidou et al. [27] designed a device to measure ion mobility in organic MIECs by studying moving front dynamics of charged species along the conducting polymer film. The problem faced was due to stability and uniformity of the invasion front due to the perturbations transverse to the propagation direction, which could be caused by, for example, variation in the MIEC film morphology.

Ion and electron transport phenomena together with electron transfer phenomena leads to coupling between the mass and charge transfer in these devices, and particularly in conductive polymer-based devices which is complex and depends on various physical and chemical properties of the materials composing the system of interest (few of them as mentioned above).

1.4 PEDOT:PSS

This thesis primarily focusses on the conducting polymer PEDOT:PSS. Poly(3,4-ethylenedioxythiophene):poly(4-styrenesulfonate) (PEDOT:PSS) is one of the most successfully commercialized conductive polymers owing to its high mechanical flexibility and excellent thermal stability [28], optical and electrical properties. PEDOT which is intrinsically conducting is stabilized in aqueous medium by counter ion poly(styrene sulfonic acid) (PSS). PEDOT:PSS finds many application such as high conductive coatings, organic LED-displays [29], as a mixed ion/electron conductor in bioelectronics, antistatic coating of polymers and glass, device electrodes, nano-fiber electrodes [30], solar cells, cathode material in electrolytic capacitors, printing wiring boards [31], textile fibers with colour changing properties [32], transparent electrodes for thick-film electroluminescence [33], source-gate-drain in the rapidly developing organic semiconductors field [34]. Due to the optical transparency (80-95%), low cost, high conducting ($>4000 \text{ S cm}^{-1}$), low sheet resistance ($<100 \text{ } \Omega \text{ sq}^{-1}$) PEDOT:PSS can be used an future alternative for ITO.

1.4.1 Structure, morphology and conduction in PEDOT:PSS

PEDOT:PSS consists of a conducting polythiophene derivative that is electrostatically bound to a PSS polyanion. The processing of PEDOT-PSS film involves formation of complex with PSS which is a counter ion that balances the charge as well as causes the dispersion of PEDOT segments in aqueous solution.

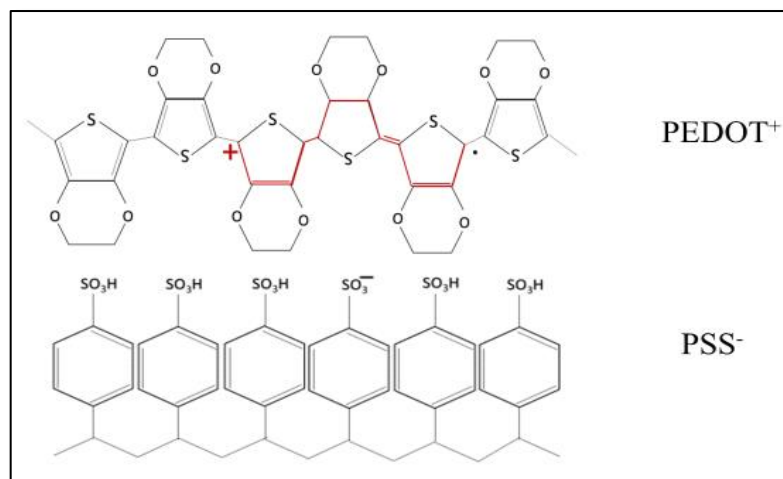


Figure (1.3): The sulfonate group in the PSS chain takes one electron from the PEDOT backbone creating a positive charge. The charge is delocalized over few monomers forming the polaron. When external voltage is applied, the polaron moves along the backbone of the PEDOT while charged sulfonate in PSS⁻ chain remains immobile.

The morphology of spin-cast PEDOT:PSS films is that of a phase segregated material consisting of PEDOT:PSS islands surrounded by a shell formed by excess PSS [35]. The conductivity of the PEDOT cores is higher than the PEDOT-depleted grain boundary, which is insulating because PSS is a weak ionic conductor. So, the conduction is obstructed near the grain boundaries. The cross-sectional AFM (X-AFM) image shows PEDOT-rich “pancakes” with a thickness of a few nanometers (~ 4- 5nm) and a diameter of a few tens of nanometers (20-25nm) separated by PSS lamellas [36]. In the normal direction, the separating barriers, that is, the PSS lamellas are quasi-continuous, whereas the separations in the lateral direction are not completely closed.

1.4.2 Hopping transport in PEDOT:PSS

The temperature-dependent a.c conductivity $\sigma(T)$ of spin coated PEDOT:PSS thin films in temperature range from 77–300 K, measured in parallel and perpendicular directions describes the conduction mechanism in the film.

$$\sigma(T) = \sigma_0 \exp \left[-\left(\frac{T_0}{T} \right)^\alpha \right] \quad \dots\dots (2)$$

where σ_0 is the conductivity pre-factor, T_0 , the characteristic temperature and $\alpha = 1/(d+1)$, d =dimensionality of conduction in Variable Range Hopping (VRH) model. The value of $\alpha = 1/4$ is observed in the parallel direction which means $d=3$, i.e., 3D VRH mechanism prevails in lateral morphology of spin-coated PEDOT:PSS. Whereas, in perpendicular direction $\alpha=1$, which implies nn-hopping (nearest neighbor hopping).

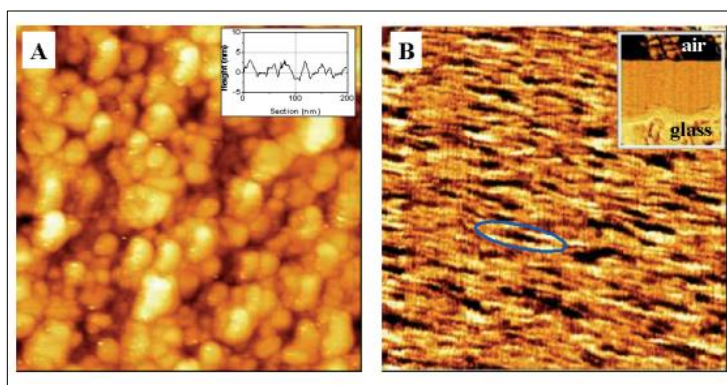
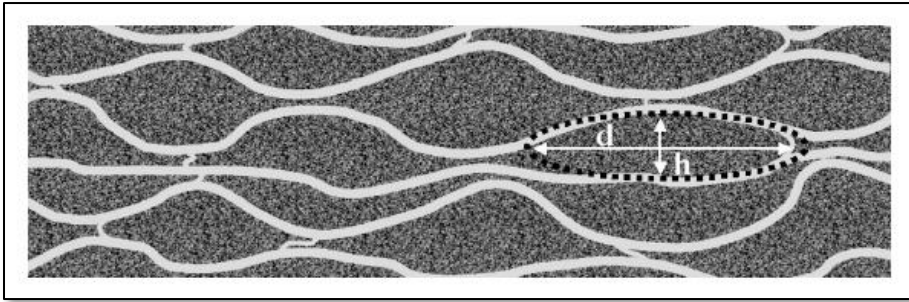


Figure 1.4. A) 200 nm \times 200 nm topographic STM image of PEDOT:PSS on indium tin oxide (ITO) at 2.3 V, tunneling current 10 pA, and vertical scale 15 nm, the inset shows a line section. B) 200 nm \times 200 nm cross-sectional AFM phase image of cleaved PEDOT:PSS on glass, vertical scale is 8°. The glass substrate is on the bottom side of the image, as shown by the inset of 530 nm \times 580 nm and vertical scale 70°. A pancake-like particle is highlighted by the ellipse. (Reprinted with permission from Ref. [36], License No. 4317630173599).



Figure(1.4c): Cross-sectional view of the schematic morphological model for PEDOT:PSS thin films derived from combined STM and X-AFM measurements. PEDOT-rich clusters (dark) are separated by lamellas of PSS (light). The PEDOT-rich lamella is composed of several pancake-like particles as pictured by the dotted lines. The typical diameter d of the particles is about 20–25 nm and the height h is about 5–6 nm. (Reprinted with permission from Ref. [36], License No. 4317630173599).

Within the PEDOT-rich lamella, the PEDOT-rich domains are only separated by the not-completely closed shells. Thus, they may either form a thin barrier, or no barrier at all, thereby allowing carriers to hop to non-nearest-neighbor sites of variable ranges. This explains 3D VRH in lateral direction. In the \perp direction (out-of plane means sandwiched structure), the PEDOT-rich domains are separated by thick barriers, formed by the PSS lamella, which show nearest-neighbor hopping and cause a reduction of conductivity. Conductivity values in out-of plane direction (10^{-6} S/cm) is off by 3-4 orders of magnitude than in lateral in-plane conductivities (10^{-3} S/cm) [36].

1.4.3 Mesoscopic 2D transport in PEDOT:PSS

PEDOT:PSS being a mixture of two different polymers seems to be different from crystalline 2D materials from the view of structural inhomogeneity, especially in drop-

cast thick films. Structural investigations and high field magnetoconductance (magnetic field $\sim 15\text{T}$) measurements have shown 2D electronic states in drop cast PEDOT:PSS films. It has been shown that charge transport in the PEDOT:PSS film can be divided into two regimes, i.e., mesoscopic 2D coherent tunneling and macroscopic 3D hopping among 2D states. 2D transport originates from the nanometer-scale self-assembled laminated structure, which is composed of PEDOT nanocrystals surrounded by insulating sheets consisting of amorphous PSSs [37].

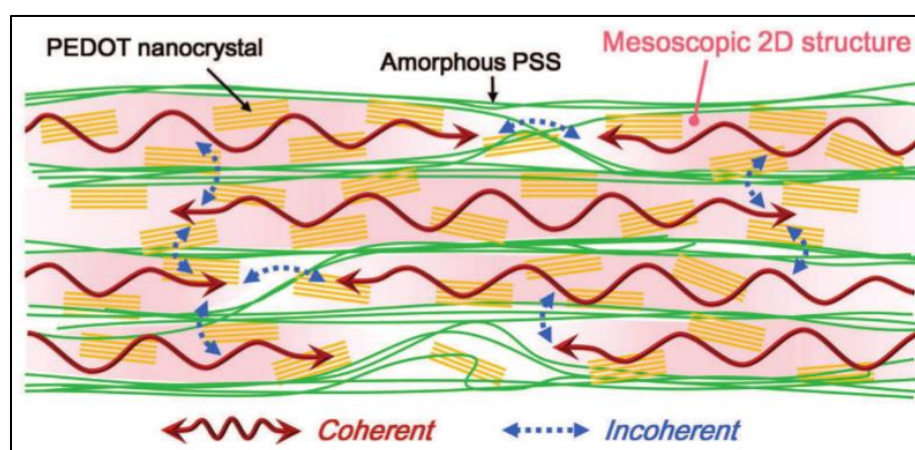


Figure (1.5): Simplified cross-sectional structure of laminated PEDOT:PSS. Pink regions indicate mesoscopic 2D structure. The red and blue arrows denote coherent and incoherent charge transport paths, respectively. (Reprinted with permission from Ref. [37], License No. 4317631179573).

The PSS chains lie parallel and are stacked perpendicular to the substrate. This stacking forms a laminated structure with a characteristic period of 3.0 nm. The PEDOT nanocrystals cling to the PSS molecules and prefer uniaxial (face-on) orientation [38,39,40].

The charge transport becomes 2D, when a charge is confined within a thin layer having a thickness less than inelastic scattering length.

1.5 Polymers in confinement

Many works have been done to investigate structure and dynamics of polymer chains in confined spaces [41,42,43]. The structure of polymers confined in cylindrical nanopores was investigated by small-angle neutron scattering [44,45] and dynamics by nuclear magnetic resonance [46,47], inelastic neutron scattering [48,49,50,51,52,53,54], dielectric spectroscopy [55,56,57] and calorimetry [58]. First, I briefly introduce the basic concepts of polymer science from the statistical mechanics point of view and then the polymer dynamics in confined channels.

1.5.1 Brief definitions from statistical point of view

The first stage of the physics of long, flexible chains was pioneered by eminent scientists such as Debye, Kuhn, Kramers, and Flory, who formulated the basic ideas. The 'classical' theory of polymer demixing, the Flory-Huggins theory, was developed in early 1940s. It is still the starting point of most current approaches – with few additions that take into account the microscopic structure of blends more accurately, or sophisticated field theories that allow to study inhomogeneous multicomponent systems of polymers with arbitrary architectures in arbitrary geometries.

The characterizing property of polymers is their modular structure. They are composed of a large number of small building blocks called monomers. The monomers are arranged in chains, which are usually flexible on the nanometer length scale. They assume a large number of conformations at room temperature since they require small energy changes to bend, stretch or form kinks. The properties of such flexible polymers are largely determined by the entropy of the chain conformations.

The fundamental processes that govern the behavior of polymeric materials do not depend on the chemical details of the monomer structure. Polymer molecules can be characterized by a few properties for qualitative purposes, such as:

- The architecture of the molecules (linear chains, rings, etc.)
- Physical properties (local chain stiffness, chain size, monomer volume)
- Physicochemical properties (monomer sequence, compatibility, charges)
- Tendency to develop crystallinity.

Few length scales relating polymeric chains are: end-to-end chain length, radius of gyration, Flory radius. These are discussed below:

A polymer chain is not a regular object and since it is subject to dynamic structural equilibrium that involves motion and further, because polymers display polydispersity in size, it is necessary to consider a statistical measure of a chain size.

For a random chain the mean size is 0, $\langle R \rangle = 0$;

(since it is equally likely to have positive and negative deviations from a chain path). Then the lowest non-zero order moment reflecting the size of a polymer chain is the second order moment about the mean chain position (or the radius of gyration). This is identical to the standard deviation about the mean for the chain length distribution, i.e.,

- $\langle R^2 \rangle = \frac{\sum_{i=1}^N (R_i - \langle R \rangle)^2}{N-1}$
- Radius of gyration, essentially the moment of inertia for a structure, for a random linear chain structure is:

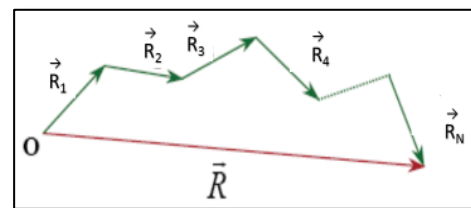


Figure (1.6): Mean size of a linear polymer chain

- $\langle R_g^2 \rangle = \frac{\langle R^2 \rangle}{6} = \frac{Na^2}{6}$; where N is the number of linear "steps" in a random polymer chain and 'a' is the length of a step.
- The Flory radius, R_F , is defined by the random walk law, $R_F = a\sqrt{N}$

1.5.2 Polymer dynamics in confinement

Confining a polymer chain leads to stretching or elongation which drives the polymer chain out of its static conformation into a stretched non-equilibrium conformation. In confined spaces, the number of available configurations for a polymer chain is reduced, leading to a free energy excess [59]. This excess free energy for an ideal linear chain, F_{id} confined in a space of characteristic size D (with $D < R_0$, where $R_0 = a\sqrt{N}$ is the natural size of the chain, N is the number of monomers and 'a' is the monomer size) is given by [60]:

$$\frac{F_{id}}{k_B T} = \left(\frac{R_0}{D} \right)^2 \quad \dots(3)$$

(where $k_B T$ is the thermal energy). This holds equally for an ideal chain confined between two walls, in a cylindrical pore or in a spherical cavity. 'D' denotes the characteristic size of confinement. Confinement can be divided into two regimes depending on geometrical nature of confinement [61]:

- (i) Weak confinement regime,
- (ii) Strong Confinement regime.

The configuration of the polymer is restricted due to confined structure but the conformation of the polymer at large length scale is not strong in Weak Confinement Regime. The free energy required for confinement is of purely entropic origin and is an extensive function of monomer number, N . In Strong Confinement Regime, the polymer chain is highly compressed and the confinement becomes stronger as chain length increases. Here, the

segmental interactions dominate the entropic cost due to the confinement and, consequently, the free energy is no longer simply proportional to N . This departure of the excess free energy from a linear dependence on N was observed for a linear polymer inside a closed cavity by Grosberg and Khokhlov [62].

Eqⁿ (3) which describes linear polymers somewhat varies for branched polymers. The exponent in eqⁿ (3) depends on spectral dimension which is a property depending on the connectivity (chemical structure of the cluster) but does not depend on the spatial conformation of the cluster. In a capillary confinement for branched polymers, it has been showed that the volume fraction of branched polymers entering the pores increases with penetration process.

According to our intuition, a polymer entering a narrow capillary will face more difficulty to penetrate. But it turns out to be that the confinement forces (the osmotic force) increase the permeation process. There is a balance between the osmotic and the hydrodynamic drag force during a polymer injection in a capillary. The hydrodynamic drag force (Stoke's drag force) is seen to assist the flow of polymer into pores more rapidly over the osmotic forces [61].

The melt diffusion of polymers confined to nanoscale cylinders has also been studied by molecular dynamics simulations and depth profiling experiments. The local dynamics of polymers confined to cylinders exhibit anisotropic relaxations. Perpendicular to the cylindrical axis, monomer motion is suppressed by the adjacent wall, while motion along the cylindrical axis is faster relative to the bulk dynamics [63].

1.6 Overview of thesis

In this thesis, the electrical transport mechanism of conducting polymer PEDOT:PSS due to confinement effects are studied. The change in carrier transport in PEDOT:PSS is effected below a characteristic length scale.

Chapter 2 deals with Materials and Methods used in the experiment. Impedance measurements (at varying temperature) using parameter analyzer, lock-in amplifier and some AFM and CAFM studies to probe the measurements at nanoscale are discussed.

The results are discussed in Chapter 3. The a.c conductivity and low-temperature studies help in deciding the transport taking place in bulk and on confinement. The optimization steps required, some calculations needed to take into account the affecting factors are briefly discussed.

Chapter 4 describes the summary of the thesis work, some improvements and simulations required to support the work. Extending this work further to study ion transport dynamics in confined channels and probe morphology variation below a characteristics length scale has been discussed.

References:

- 1) A.G. MacDiarmid, "A novel role for organic polymers," *Angew Chem Int.*, vol. 40, pp. 2581-2590, 2001
- 2) H. Shirakawa, "The discovery of polyacetylene film: the dawning of an era of conducting polymers (Nobel Lecture)," *Angew Chem Int.*, vol. 40, pp. 2574-2580, 2001.
- 3) A.J. Heeger, "Semiconducting and metallic polymers: the fourth generation of polymeric materials (Nobel Lecture)," *Angew Chem Int.*, vol. 40, pp. 2591-2611, 2001.
- 4) *Conducting Polymers: Synthesis, Properties and Applications; International Advanced Research Journal in Science, Engineering and Technology Vol. 2, Issue 11, 2015*
- 5) C.W. Tang, S.A. Vanslyke, *Appl. Phys. Lett.* 51 (12), 913 (1987)
- 6) R.H. Friend, R.W. Gymer, A.B. Holmes, J.H. Burroughes, R.N. Marks, C. Taliani, D.D.C. Bradley, D.A. Dos Santos, J.L. Bredas, M. Logdlund, W.R. Salaneck, *Nature* 397 (6715), 121 (1999)

- 7) Berggren, M. & Richter-Dahlfors, A. Organic bioelectronics. *Advanced Materials* 19, 3201-3213 (2007)
- 8) Z.T. Zhu, J.T. Mabeck, C.C. Zhu, N.C. Cady, C.A. Batt, G.G. Malliaras, *Chem. Commun.* (13),1556 (2004).
- 9) D.A. Bernards, D.J. Macaya, M. Nikolou, J.A. DeFranco, S. Takamatsu, G.G. Malliaras, *J.Mater. Chem.* 18 (1), 116 (2008)
- 10) Bernards, D. A. & Malliaras, G. G. Steady-state and transient behavior of organic electrochemical transistors. *Adv. Funct. Mater.* 17, 3538–3544 (2007)
- 11) J. Y. Wong, R. Langer and D. E. Ingber, Electrically conducting polymers can noninvasively control the shape and growth of mammalian cells, *Proc. Natl. Acad. Sci. U. S. A.*, 1994, 91, 3201–3204
- 12) C. Salto, E. Saindon, M. Bolin, A. Kancierzewska, M. Fahlman, E. W. H. Jager, P. Tengvall, E. Arenas and M. Berggren, Control of neural stem cell adhesion and density by an electronic polymer surface switch, *Langmuir*, 2008, 24, 14133–14138
- 13) J. Makinen, I. G. Hill, R. Shashindhar, N. Nikolov, Z. H. Kafafi; *Appl. Phys. Lett.* 2001,79, 557
- 14) Kroschwitz, J.I.; Winokur, M, *J. Chem. Educ.*, 1988, 65 (6), p A168
- 15) Riess I. Mixed ionic–electronic conductors material properties and applications. *Solid State Ionics.* 2003;157(1):1–17
- 16) Crone B, Dodabalapur A, Gelperin A, Torsi L, Katz HE, Lovinger AJ, Bao Z. Electronic sensing of vapors with organic transistors. *Appl Phys Lett.* 2001;78(15):2229–2231
- 17) Chang JB, Liu V, Vivek S, Sivula K, Luscombe C, Murphy A, Liu J, Fréchet JMJ. Printable polythiophene gas sensor array for low-cost electronic noses. *J Appl Phys.* 2006;100(1):014506
- 18) Pei Q, Yu G, Zhang C, Yang Y, Heeger AJ. Polymer light-emitting electrochemical cells. *Science.* 1995;269(5227):1086–1088

- 19) van Reenen S, Matyba P, Dzwilewski A, Janssen RAJ, Edman L, Kemerink M. A unifying model for the operation of light-emitting electrochemical cells. *J Am Chem Soc.* 2010;132:13776–13781.
- 20) Schön JH, Dodabalapur A, Bao Z, Kloc C, Schenker O, Batlogg B. Gate-induced superconductivity in a solution-processed organic polymer film. *Nature.* 2001;410(6825):189–192
- 21) Frackowiak E, Khomenko V, Jurewicz K, Lota K, Beguin F. Supercapacitors based on conducting polymers/nanotubes composites. *J Power Sources.* 2006;153(2):413–418
- 22) Koezuka H, Tsumura A, Ando T. Field-effect transistor with polythiophene thin film. *Synth Met.* 1987;18(1):699–704
- 23) Cramer T, Campana A, Leonardi F, Casalini S, Kyndiah A, Murgia M, Biscarini F. Water-gated organic field effect transistors—opportunities for biochemical sensing and extracellular signal transduction. *J Mater Chem B.* 2013;1(31):3728–3741
- 24) Leger JM. Organic electronics: the ions have it. *Adv Mater.* 2008;20(4):837–841
- 25) White HS, Kittleson GP, Wrighton M. Chemical derivatization of an array of three gold microelectrodes with polypyrrole: fabrication of a molecule-based transistor. *J Am Chem Soc.* 1984;106(18):5375–5377
- 26) Borsenberger PM, Weiss DS. *Organic Photoreceptors for Xerography.* New York: Marcel Dekker, 1998.
- 27) Stavrinidou E, Leleux P, Rajaona H, Khodagholy D, Rivnay J, Lindau M, Sanaur S, Malliaras GG. Direct measurement of ion mobility in a conducting polymer. *Adv Mater.* 2013;25:4488–4493.
- 28) Wang, Research progress on a novel conductive polymer-poly(3,4-ethylenedioxythiophene) (PEDOT), *J. Phys.: Conf. Ser.*, 2009, 152, 012023
- 29) N. Koch, A. Vollmer, A. Elschner, *Appl. Phys. Lett.* 90 (2007) 043512
- 30) M.H. Bolin, K. Svennersten, X. Wanga, I.S. Chronakis, A. Richter-Dahlfors, E.W.H Jager, M. Berggren, *Sens. Actuators, B* 142 (2009) 451

- 31) J. Hupe, G.D. Wolf, F. Jonas, *Galvanotechnik* 86 (1995) 3404
- 32) A. Laforgue, *J. Mater. Chem.* 20 (2010) 8233
- 33) N. Koch, A. Kahn, J. Ghijsen, J.-J. Pireaux, J. Schwartz, R.L. Johnson, A. Elschner, *Appl. Phys. Lett.* 82 (2003) 70
- 34) M. Halik, H. Klauk, U. Zschieschang, G. Schmid, W. Radlik, S. Ponomarenko, S. Kirschmeyer, *J. Appl. Phys.* 93 (2003) 2977
- 35) X. Crispin, S. Marciniak, W. Osikowicz, G. Zotti, A. W. Denier van der Gon, F. Louwet, M. Fahlman, L. Groenendaal, F. de Schryver, W. R. Salaneck, *J. Polym. Sci. Part B: Polym. Phys.* 2003, 41, 2561
- 36) Alexandre Mantovani Nardes et al., *Microscopic Understanding of the Anisotropic Conductivity of PEDOT:PSS Thin Films*, *Adv. Mater.* 2007, 19, 1196–1200
- 37) Yuta Honma ,*Mesoscopic 2D Charge Transport in Commonplace PEDOT:PSS Films*, *Adv. Electron. Mater.* 2018, 4, 1700490.
- 38) C. M. Palumbiny, F. Liu, T. P. Russell, A. Hexemer, C. Wang, P. Müller-Buschbaum, *Adv. Mater.* 2015, 27, 3391
- 39) Q. Wei, M. Mukaida, Y. Naitoh, T. Ishida, *Adv. Mater.* 2013, 25, 2831
- 40) O. Bubnova, Z. U. Khan, H. Wang, S. Braun, D. R. Evans, M. Fabretto, P. Hojati-Talemi, D. Dagnelund, J. Arlin, Y. H. Geerts, S. Desbief, D. W. Breiby, J. W. Andreasen, R. Lazzaroni, W. M. Chen, I. Zozoulenko, M. Fahlman, P. J. Murphy, M. Berggren, X. Crispin, *Nat. Mater.* 2013, 13, 190
- 41) de Gennes, P.-G. *Scaling Concepts in Polymer Physics*; Cornell University Press: Ithaca, NY, 1979
- 42) Vilgis, T. A. *Phys. Rep.* 2000, 336, 167.
- 43) *Structure and Dynamics of Confined Polymers*; Kasianowicz, J. J., et al. Eds.; Kluwer Academic Publishers: Dordrecht, The Netherlands, 2002.
- 44) Shin, K.; Obukhov, S.; Chen, J. T.; Huh, J.; Hwang, Y.; Mok, S.; Dobriyal, P.; Thiagarajan, P.; Russell, T. P. *Nat. Mater.* 2007, 6 (12), 961–965.

- 45) Noirez, L.; Stillings, C.; Bardeau, J. F.; Steinhart, M.; Schlitt, S.; Wendorff, J. H.; Pepy, G. *Macromolecules* 2013, 46 (12), 4932–4936
- 46) Ok, S.; Steinhart, M.; Serbescu, A.; Franz, C.; Chavez, F. V.; Saalwachter, K. *Macromolecules* 2010, 43 (10), 4429–4434
- 47) Hofmann, M.; Herrmann, A.; Ok, S.; Franz, C.; Kruk, D.; Saalwachter, K.; Steinhart, M.; Rossler, E. A. *Macromolecules* 2011, 44(11), 4017–4021.
- 48) Krutyeva, M.; Martin, J.; Arbe, A.; Colmenero, J.; Mijangos, C.; Schneider, G. J.; Unruh, T.; Su, Y. X.; Richter, D. *J. Chem. Phys.* 2009, 131 (17), 174901.
- 49) Kusmin, A.; Gruener, S.; Henschel, A.; de Souza, N.; Allgaier, J.; Richter, D.; Huber, P. *Macromolecules* 2010, 43 (19), 8162–8169.
- 50) Kusmin, A.; Gruener, S.; Henschel, A.; Holderer, O.; Allgaier, J.; Richter, D.; Huber, P. *J. Phys. Chem. Lett.* 2010, 1 (20), 3116–3121.
- 51) Lagrene, K.; Zanotti, J. M.; Daoud, M.; Farago, B.; Judeinstein, P. *Eur. Phys. J.-Spec. Top.* 2010, 189 (1), 231–237.
- 52) Lagrene, K.; Zanotti, J. M.; Daoud, M.; Farago, B.; Judeinstein, P. *Phys. Rev. E* 2010, 81 (6), 060801.
- 53) Martin, J.; Krutyeva, M.; Monkenbusch, M.; Arbe, A.; Allgaier, J.; Radulescu, A.; Falus, P.; Maiz, J.; Mijangos, C.; Colmenero, J.; Richter, D. *Phys. Rev. Lett.* 2010, 104 (19), 197801
- 54) Krutyeva, M.; Wischnewski, A.; Monkenbusch, M.; Willner, L.; Maiz, J.; Mijangos, C.; Arbe, A.; Colmenero, J.; Radulescu, A.; Holderer, O.; Ohl, M.; Richter, D. *Phys. Rev. Lett.* 2013, 110 (10), 119901.
- 55) Schonhals, A.; Goering, H.; Schick, C. *J. Non-Cryst. Solids* 2002, 305 (1–3), 140–149
- 56) Kremer, F.; Schonhals, A. *Broadband Dielectric Spectroscopy*; Springer: Berlin, Germany, 2003
- 57) Schonhals, A.; Goering, H.; Schick, C.; Frick, B.; Zorn, R. *J. Non-Cryst. Solids* 2005, 351 (33–36), 2668–2677
- 58) Schonhals, A.; Goering, H.; Schick, C.; Frick, B.; Mayorova, M.; Zorn, R. *Eur. Phys. J.-Spec. Top.* 2007, 141, 255–259

59) Daoud, M.; de Gennes, P.-G. *J. Phys. (Paris)* 1977, 38, 85

60) Cassasa, E. F. *J. Polym. Sci.* 1967, B5, 773

61) Takahiro Sakaue, *Polymer Chains in Confined Spaces and Flow-Injection Problems: Some Remarks*, *Macromolecules*, Vol. 39, No. 7, 2006

62) Grosberg, A. Yu.; Khokhlov, A. R. *Statistical Physics of Macromolecules*, American Institute of Physics: New York, 1994

63) Wei-Shao Tung et al., *Local Polymer Dynamics and Diffusion in Cylindrical Nanoconfinement*, *Macromolecules* 2015, 48, 2324–2332

CHAPTER 2

MATERIALS AND METHODS

This chapter describes the materials required for fabrication of device and experimental techniques used to study the vertical transport of a conducting polymer in confined channels.

2.1 Materials:

Sample preparation requires following materials: transparent conducting electrode ITO substrate ($7\Omega/\square$), highly conducting polymer PEDOT:PSS (Clevios™ AI 4083), Ultrathin Anodic Aluminium Oxide membrane AAO (purchased from TopMembranes Technology) of different pore diameters 20 nm, 50 nm, 100 nm, 340 nm.

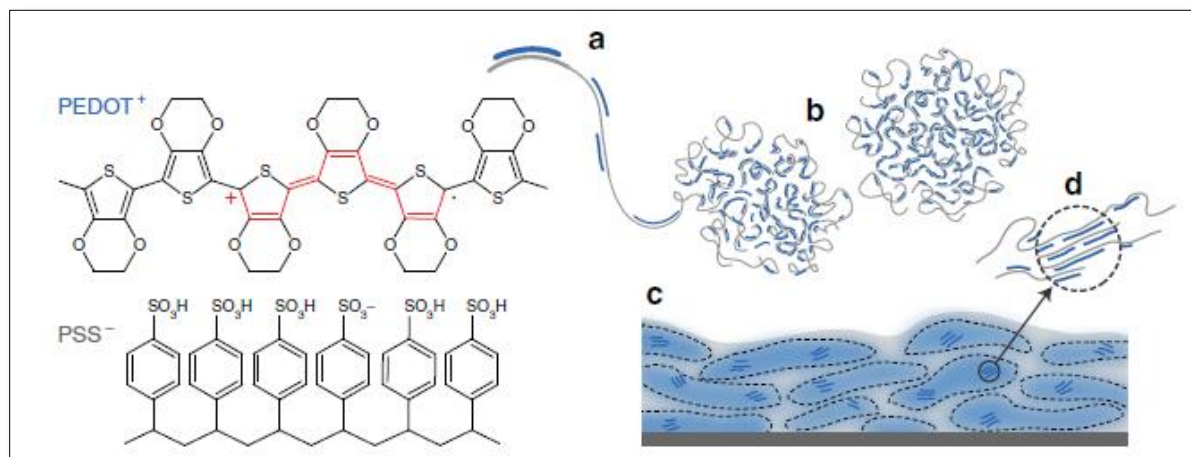
2.1.1 PEDOT:PSS

Poly(3,4-ethylenedioxythiophene) doped with poly(styrenesulfonate), PEDOT:PSS, has been utilized for over two decades as a stable, solution-processable hole conductor. PEDOT which is intrinsically conducting is stabilized in aqueous medium by counter ion poly(styrene sulfonic acid) (PSS). While its hole transport properties have been the subject of intense investigation, recent work has turned to PEDOT:PSS as a mixed ionic/electronic conductor in applications including bioelectronics, energy storage and management, and soft robotics [1]. This polymer has been introduced here to study its mixed ion/electron transport in confined space.

For this thesis work, two grades of PEDOT:PSS has been used (purchased from Ossila), namely- (i) AI4083 grade and (ii) PH1000 grade.

AI4083 grade is generally used as buffer layer in organic light emitting diodes (OLEDs) and photovoltaics. PEDOT:PSS content is 1:6. PSS is a polyelectrolyte that is lightly doped with

Na. Work function PEDOT:PSS of this grade is around 5.0 - 5.2 eV. Whereas PH1000 is high conducting grade polymer which is used as electrodes/interfacial films and applications which demand for high conductivity. PEDOT:PSS content is 1:2.5 and its work function is slightly less than Al4083 grade, i.e., 4.8 – 5.0 eV .



Figure(2.1) : *PEDOT:PSS structure and morphology. (a) synthesis onto PSS template, (b) formation of colloidal gel particles in dispersion and (c) resulting film with PEDOT:PSS-rich (blue) and PSS-rich (grey) phases. (d) Aggregates/crystallites support enhanced electronic transport. (Reprinted with permission from Ref.[1] under Creative Commons Attribution 4.0 International License).*

2.1.2 Ultrathin AAO membranes

Ultrathin Anodic Aluminum Oxide (AAO) templates are ordered arrays of surface nanostructures. Pores of ultrathin AAO template are uniform in diameter and highly ordered in a short-range. In addition, the material (Al_2O_3) is transparent in the near-infrared and visible spectrum and is electrically insulated. Ultrathin AAO template has special

advantages such as large pattern area ($>1 \text{ cm}^2$), high throughput, ultrahigh density (10^8 – 10^{12} pores/ cm^2) of the surface nanostructures.

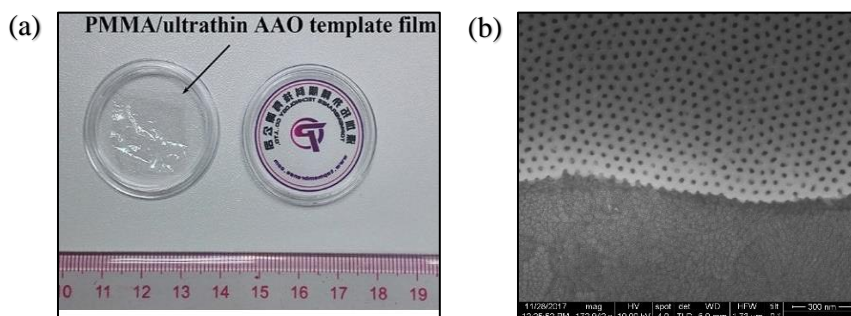


Figure (2.2): Ultrathin AAO template (a) product of ultrathin AAO template in standard size ($15 \times 15 \text{ mm}$) [2], (b) SEM image of 20nm AAO on ITO.

Each vertical pore (thickness $\sim 200 \text{ nm}$) in the AAO template acted as nano- (or meso) confined space for the polymer introduced in it. The transport through each pore (along the length of 200 nm) doesn't interfere with adjacent pores due to insulating Al_2O_3 walls.

2.1.3 Additive (DMSO)

The addition of co-solvent dimethyl sulfoxide (DMSO) increases the conductivity and modifies the dielectric response as observed from the literature. Also, the surface roughness and morphology change with composition of PEDOT:PSS : DMSO and film deposition conditions.

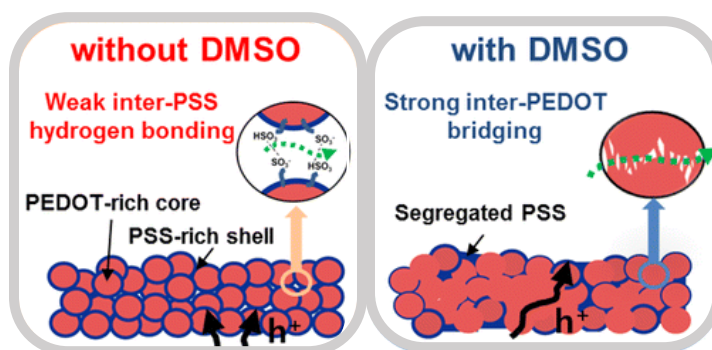


Figure (2.3): Schematic model of structural modification in PEDOT:PSS with the addition of co-solvents[3].(Reprinted with permission from Ref[3] Copyright (2016) American Chemical Society.)

In the PEDOT:PSS film without any co-solvent, the PEDOT nanocrystals are embedded in the PSS matrix with the PSS chain network largely aligned along the surface. The higher number of PSS chains on the surface reduces the ohmic contact points. Addition of a co-solvent increases packing density of PEDOT and produces clustering with reduced PSS content at the surface [4]. Here, DMSO is added in proportions with PEDOT:PSS and introduced in the pores of AAO which shows a decrease in conductivity that is opposite to the behavior as observed in bulk.

2.2 Device Fabrication and characterization

The following section describes the steps of sample preparation and experimental techniques to characterize them.

AAO membranes were transferred onto RCA cleaned etched ITO substrates. The sample was then dip coated with PEDOT:PSS. Conc. HCl and Zn powder were used to etch ITO to the desired pattern.

RCA process include four steps *viz*,

- (i) ultrasonic cleaning in soap solution (5-10% extran solution in deionized water) at elevated temperature (60°C for 10 min.),

- (ii) washing followed by ultrasonication in deionized water(10 min.) and drying in nitrogen flow.
- (iii) ultra sonic cleaning in Isopropyl alcohol : Acetone mix (1:1) for 10 min and
- (iv) cleaning in Ammonia: H₂O₂: water (1:1:5 mixture) at 100°C till all the bubbles emerging from the samples stops. Substrates were then rinsed in deionized water and dried under ultra-high pure nitrogen flow.

Transferring AAO on ITO substrates:

- (i) The cleaned ITO substrate is made hydrophilic using plasma treatment.
- (ii) The AAO membrane is placed on the substrate with AAO side facing to the substrate.
- (iii) PMMA base support is removed in acetone bath.

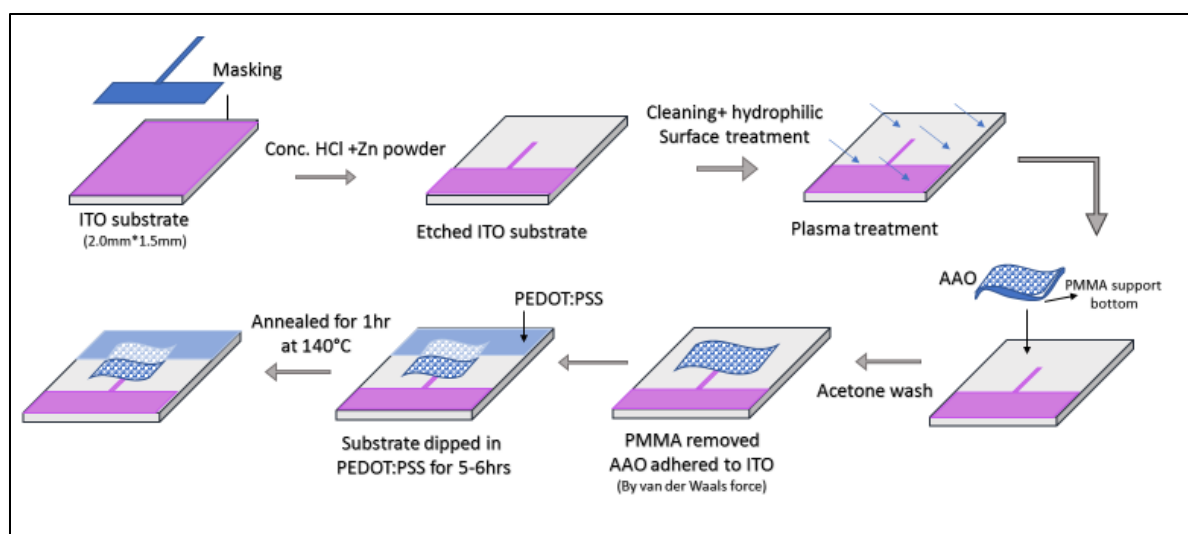
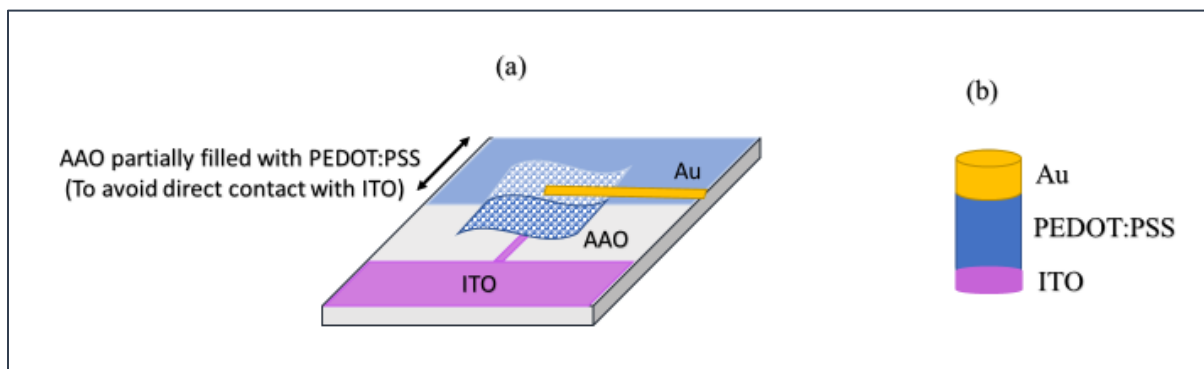


Figure (2.4) : Steps involved in preparation of sample .

After transferring the AAO membrane, the substrate is once again subjected to plasma treatment for ~30s. The substrate is instantaneously dipped in PEDOT:PSS solution (Clevios™ AI 4083) for about 5-6 hrs. The sample is then annealed for 1hr at 140 °C.

For AFM and CAFM studies the sample designed in figure (2.4) is used. The CAFM tips are coated with Au, so a top conducting layer is not required. But for macroscopic measurements, like impedance spectroscopy, voltage switching analysis, the sample in Figure (2.4) is coated with top layer of Au (100 nm) using Physical Vapor Deposition.



Figure(2.5): (a) Au coating on the PEDOT:PSS filled nanopores. (b) Schematic of effective one pore structure.

The coating should be sufficient for the sample to be conducting such that a vertical transport can be probed. The thickness of Au to be coated can be known from AFM morphology image. AFM images show ~ 50-60 nm roughness. So, an gold coating of 65-70 nm is deposited on the membranes for experimental studies.

With additives: -

The same is repeated for samples prepared with DMSO in PEDOT:PSS. Different proportions of DMSO is added to fixed volume of PEDOT:PSS.

- (a) 10wt % DMSO in PEDOT:PSS, (b) 20wt % DMSO in PEDOT:PSS and (c) 30wt% DMSO in PEDOT:PSS.

Ethylene Glycol, another co-solvent has also been used.

2.3 Instruments and sample characterization

(1) AFM (Atomic Force Microscopy)

The atomic force microscope is one of the variant of scanning probe microscopes. The AFM uses a flexible cantilever as a type of spring to measure the force between the tip and the sample. The basic idea of an AFM is that the local attractive or repulsive force between the tip and the sample is converted into a bending, or deflection, of the cantilever. The cantilever is attached to some form of rigid substrate that can be held fixed and depending whether the interaction at the tip is attractive or repulsive, the cantilever will deflect towards or away from the surface [5].

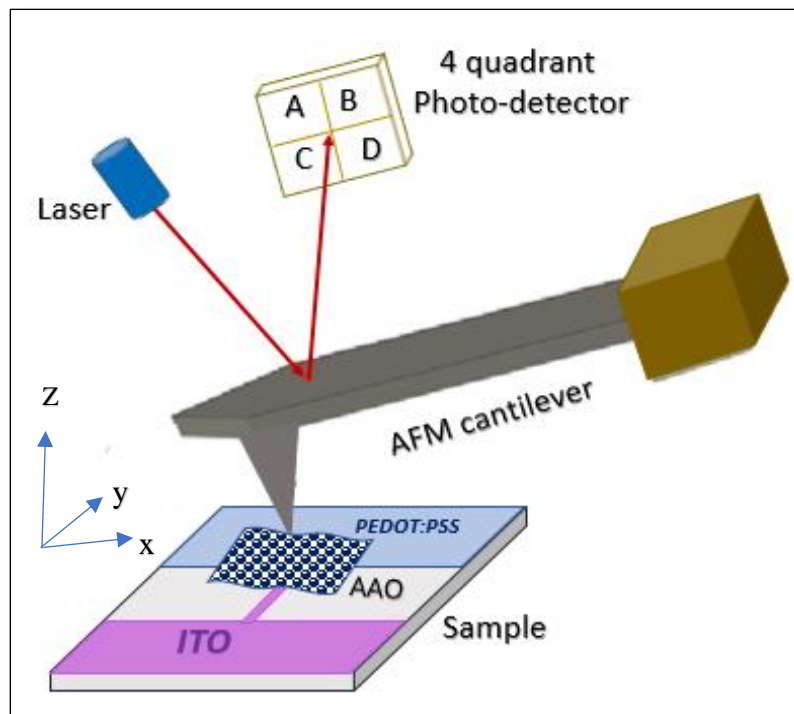


Figure (2.6). Schematic diagram of Atomic Force Microscopy.

The imaging modes in AFM are pictured in terms of the forces between the tip and surface. Two objects when brought together, the long-range forces are attractive, and becomes repulsive when the objects are close together. The longer-range attractive forces are usually van der Waals forces and capillary forces. Repulsive interaction takes over at short ranges, when the objects are in “contact” and the electron orbitals begin to overlap.

A general curve can be drawn for the tip-sample force against distance, and the different operating modes can be matched with different parts of the curve.

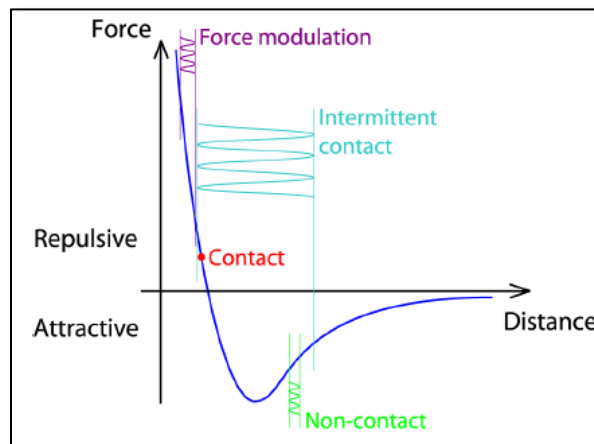


Figure (2.7). Operating regimes for the different imaging mode [1].

- **Cantilever tip used:** For studying surface morphology of the samples, Non-Contact mode tip (from NanoWorld) is used.
- **Specifications:** Thickness: 4.6 μm / Length: 160 μm / Width: 45 μm , Resonance frequency: 285 kHz / Force constant: 42 N/m.

This tip is not in contact with the surface of sample. The cantilever is usually driven close to a resonance of the system, to give a reasonable amplitude for the oscillation and also to provide phase information.

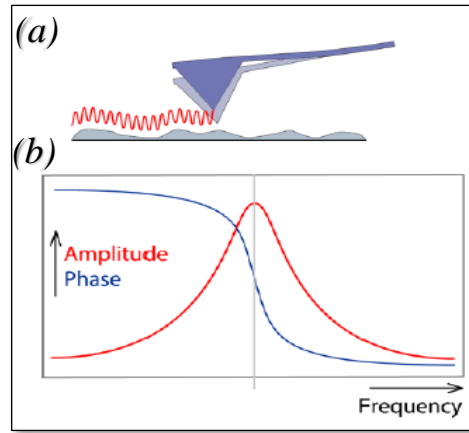


Figure (2.8) (a) Non-contact mode tip (b) Setpoint at the intersection of phase and amplitude.

PEDOT:PSS polymer coating on AAO porous membrane is made thin <200 nm so as to ensure morphology in porous membranes and not of the PEDOT:PSS alone.

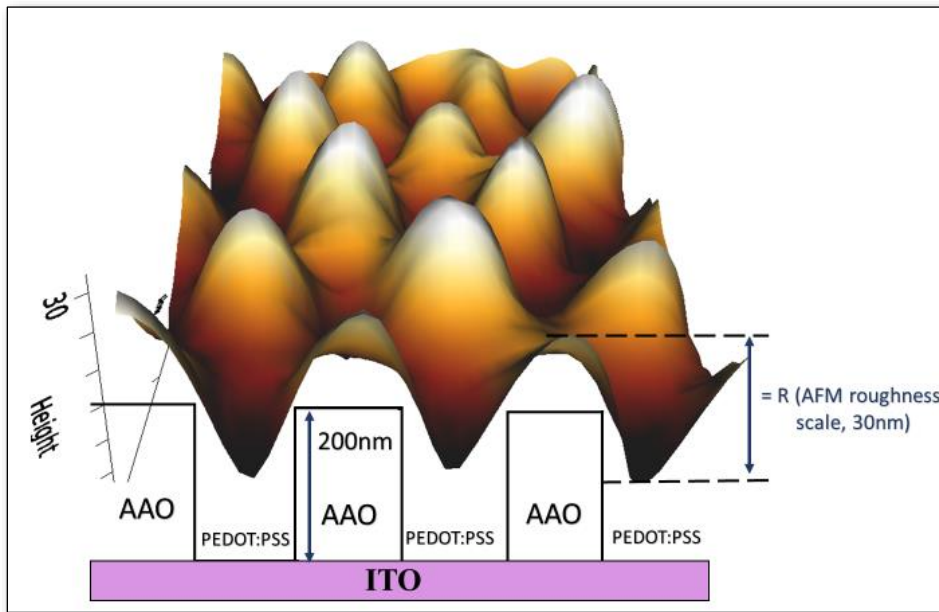


Figure (2.4) 3D image of surface morphology of 50nm pore (interpore diameter =100nm) AAO membrane showing partial filling of PEDOT:PSS into the pores (not to scale).

(2) Conductive Atomic Force Microscopy (CAFM)

Measuring local properties of the sample increases the accuracy of the measurement over bulk property values. Using Conductive AFM, one can simultaneously measure topography and current distribution (conductivity) over the desired sample surface by using Au/Pt coated AFM tip as a nanometer-scale electrical probe [6].

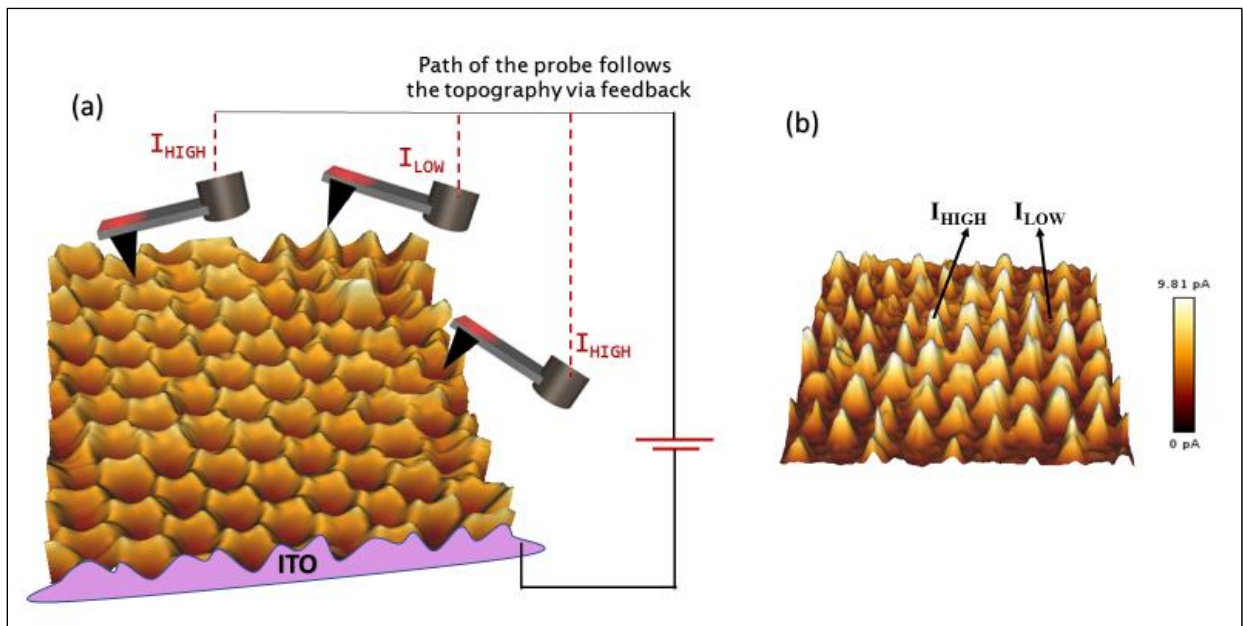


Figure (2.9) Schematic diagram of CAFM system. (a) Topography of PEDOT:PSS filled AAO surface, (b) Current profile obtained after CAFM scan.

In CAFM scan, a bias voltage is applied between conducting tip and sample and the tunneling current between the two is measured. Conductive cantilever scans the sample surface in contact mode to produce a topography map and the electric current between the cantilever and the sample is measured simultaneously (Figure 2.5). Since electric current

through the conducting cantilever can be as small as a pA, the current amplifier is chosen so that the electrical noise is suppressed on ~ fA.

- **Cantilever tip used:** Au coated Contact mode tip (dimension 25 nm).
- **Specifications:** Thickness: 2 μm / Length: 450 μm / Width: 50 μm, Resonance Frequency: 13kHz / Force constant: 0.2 N/m.

The AAO membrane transferred onto ITO substrate is not uniform throughout the sample. Fractures and undulations occur in some regions. Since the contact size of AFM cantilever tip ~few nanometers, local current distribution through each pore can be obtained conveniently avoiding the cracks and fractures which may otherwise be due to the bulk transport.

(3) Impedance Spectroscopy

Electrochemical impedance is a response of an electrochemical system to an applied electric potential. Electrochemical impedance is measured using a small excitation signal (small amplitude ~10mV, 30 mV AC ripple on top of a controlled DC potential). This is to ensure that the system response is in linear region. In a linear system, the current response will be sinusoidal to the applied sinusoidal potential at the same frequency but shifted in phase (in degrees).

Applied potential field to the system: $V = V_0 \sin\omega t$

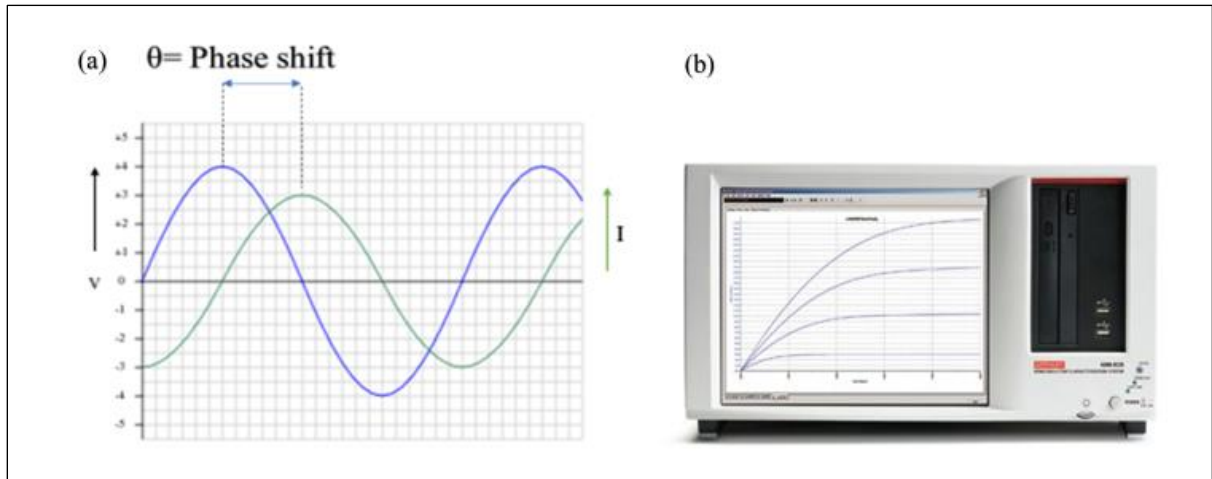


Figure (2.10): (a) Current response in a linear system, (b) 4200SCS Semiconductor parameter analyzer.

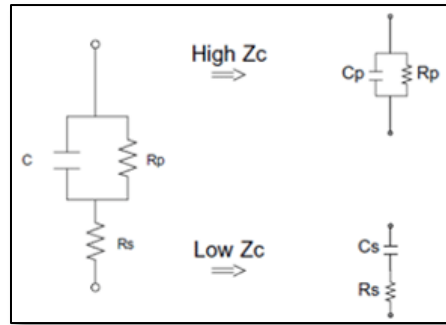
In a linear system, the response current, I , is shifted by phase (θ) and has an amplitude different than I_0 :

$$I = I_0 \sin(\omega t + \theta)$$

$$\text{Impedance of the system, } Z = \frac{V}{I} = \frac{V_0 \sin \omega t}{I_0 \sin(\omega t \pm \theta)}$$

$$\text{In Euler's notation, } Z = \frac{V_0 e^{i\omega t}}{I_0 e^{i(\omega t - \theta)}} = Z_0 e^{i\theta} = Z_0 (\cos\theta + i\sin\theta)$$

There are two common AC impedance models in parameter analyzer: the parallel model and the series model. In the parallel model, results are expressed as the parallel capacitance (C_p) and the parallel conductance (G_p). In the series model, results are expressed as the series capacitance (C_s) and the series resistance (R_s). Usually C_s is calculated for impedance $< 10 \Omega$. In the system used in experiment, impedance is greater than 10Ω , so C_p and $G_p = 1/R_p$ values are used.



Figure(2.12) Equivalent circuit for C_p , G_p , C_s , G_s .

From impedance measurement, the a.c conductivity is analyzed as a function of varying temperature (from -150°C to 150°C) and frequency. Semiconductor Parameter Analyzer 4200 SCS is used for measuring impedance from frequencies 10kHz to 10MHz. For low frequencies measurements lock-in amplifier SR830 is used.

(4) Low-Temperature measurements

A.c conductivity is performed at low temperatures using LINKAM setup. This contains a closed sample chamber which is connected to parameter analyzer for measuring impedance. The LINKAM setup provides nitrogen environment inside the chamber. The chamber is initially purged for around 30min to ensure complete moisture free nitrogen environment inside the sample chamber.

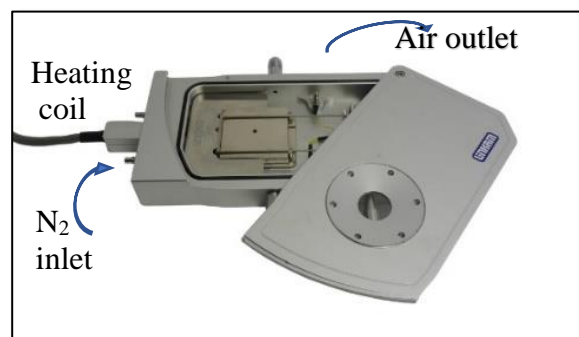


Figure (2.13) LINKAM sample stage

References:

1. Jonathan Rivnay, Sahika Inal, Eleni Stavrinidou, George G. Malliaras, Structural control of mixed ionic and electronic transport in conducting polymers, *Nature Communications*, 7:11287
2. *TopMembrane Ultrathin AAO(products)*
3. Inhwa Lee†‡, Gun Woo Kim†, Minyang Yang†, and Taek-Soo Kim, Simultaneously Enhancing the Cohesion and Electrical Conductivity of PEDOT:PSS Conductive Polymer Films using DMSO Additives, *ACS Appl. Mater.Interfaces*, 2016 , 8 (1) , pp 302–310
4. Joseph Palathinkal Thomas , Liyan Zhao , Donald McGillivray and Kam Tong Leung, High-efficiency hybrid solar cells by nanostructural modification in PEDOT:PSS with co-solvent addition, *J. Mater. Chem. A*, 2014, 2, 2383-2389
5. JPK Nanowizrd handbook
6. Nanotechnology Solutions Partner (Mode Note)

CHAPTER 3

RESULTS AND DISCUSSIONS

This chapter describes the experimental results obtained from measurements done in bulk sample and on confinement. First, measurements in bulk are done and then the electrical transport studies are investigated in confined channels.

3.1 Measurements in bulk PEDOT:PSS

Measurements for d.c and a.c conductivity are done for thin film PEDOT:PSS.

3.1.1 D.C Conductivity

(1) Pristine PEDOT:PSS (Al4083 grade)

Heraeus Clevios™ Al4083 grade (low conducting grade polymer), most commonly used PEDOT:PSS formulations is often used for matching of interfacial energy levels in thin film electronic devices due to its deep work function [1]. PEDOT:PSS content is 1:6. The polymer is pre-filtered using 2.5 μ m filter paper and spin-coated at ~500 rpm on plasma cleaned ITO surface (7 Ω/\square). It is then annealed for 1hr at 140 °C (same cleaning and annealing procedure followed as mentioned in section 2.3). Top Au electrode is thermally evaporated with a thickness of ~40nm. Parameter Analyzer 4200 SCS is used to measure I-V characteristics of the sandwiched structure of PEDOT:PSS.

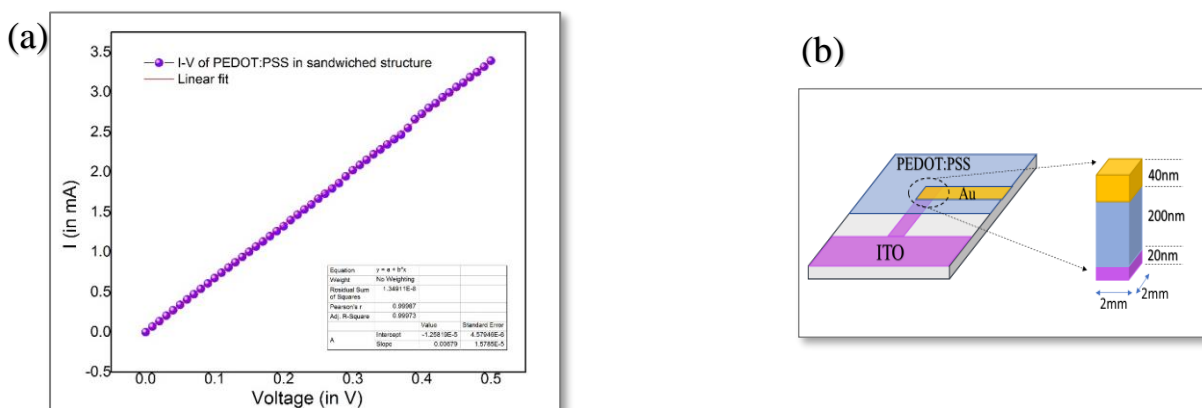


Figure (3.1): (a) I-V curve of PEDOT:PSS for vertical (out-of-plane) transport.

(b) Sandwiched device structure for graph(a).

➤ Calculation of out-of-plane conductivity:

The device in figure (3.1 b) is swept from 0V to 0.5V. Since PEDOT:PSS forms ohmic contact, I-V curve is linear as expected.

Following Ohm's law; $V = IR$,

$$\Rightarrow V = I * \rho * \frac{l}{A}$$

$$\Rightarrow \rho = \frac{V * A}{I * l}$$

$$\Rightarrow \sigma_{d.c} = \frac{I * l}{V * A} = \frac{l}{R * A}$$

The thickness of film, $l \sim 200\text{nm}$ (known from AFM surface roughness), Area of contact,

$$A \sim 2\text{mm} * 2\text{mm}. \text{ Resistance, } R \sim \frac{1}{\text{slope of } I-V} = \frac{1}{0.0067} = 144.92\Omega$$

$$\therefore \sigma_{d.c} = 3.45 * 10^{-6} \text{ S/cm} \quad \dots (3.1)$$

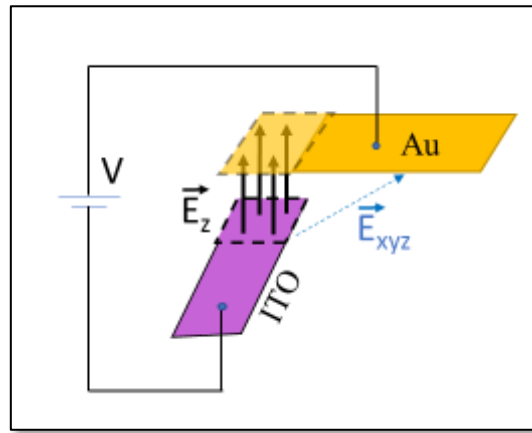


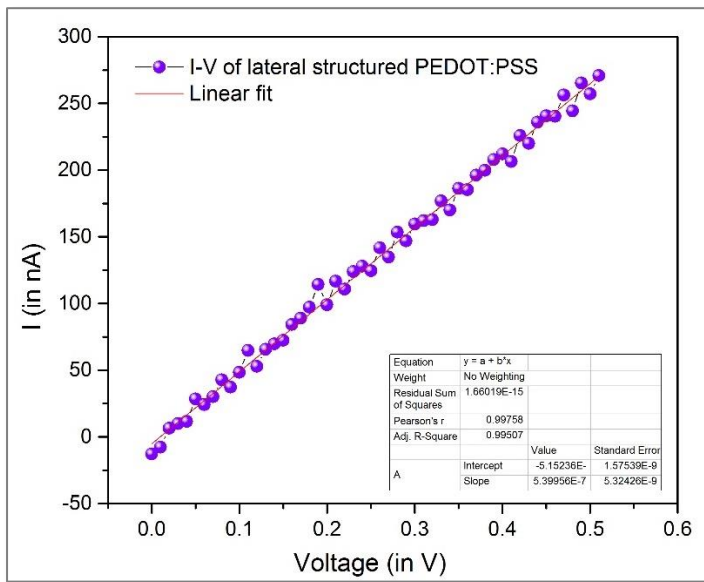
Figure (3.2): The electric field lines like \vec{E}_z contribute to current. Lines like \vec{E}_{xyz} which are not perpendicular to the overlapping electrodes have small magnitudes compared to \vec{E}_z and thus are neglected.

For in-plane conductivity, four Au strips (separated by 80 μm) of dimension 1mm x5mm and thickness ~40nm was deposited on spin coated PEDOT:PSS (~40 nm) on cleaned glass surface.

Four-probe measurements was used to find the sheet resistivity. Let the thickness of film be ‘t’ and Au strips are separated by ‘s’ distance.

For a thin film , if $t \ll s$, Resistivity, $\rho = \frac{\pi t}{\ln 2} \frac{V}{I} = 4.53 \frac{V}{I} t$

(a)



(b)

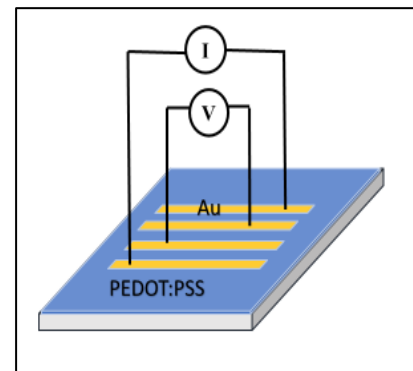


Figure (3.3): (a) I-V curve of PEDOT:PSS for lateral (in-plane) transport. (b) Device structure (four probe setup) for graph(a).

➤ **Calculation of in-plane conductivity :**

For the device structure used, $\frac{t}{s} = \frac{40nm}{80\mu m} \sim 10^{-4} \Rightarrow t \ll s$.

$$\rho = 4.53 \frac{V}{I} t = 4.53 \frac{1}{\text{slope of I-V}} t = 4.53 \frac{1}{5.399E-7} t$$

$$\Rightarrow \sigma_{d.c} = 2.9 * 10^{-2} \text{ S/cm} \quad \dots (3.2)$$

In-plane (lateral) conductivity of PEDOT:PSS is higher by 3-4 orders of magnitude compared to out-of plane conductivity.

(2) *Pristine PEDOT:PSS (PH1000 grade)*

PH1000 grade of PEDOT:PSS is used for applications where high conductivity is required. It has very low sheet resistance (~300Ω/□). PEDOT:PSS content is 1: 2.5. The polymer is first pre-filtered with 2.5μm and same preparation procedure is followed as mentioned in previous section (3.1.1).

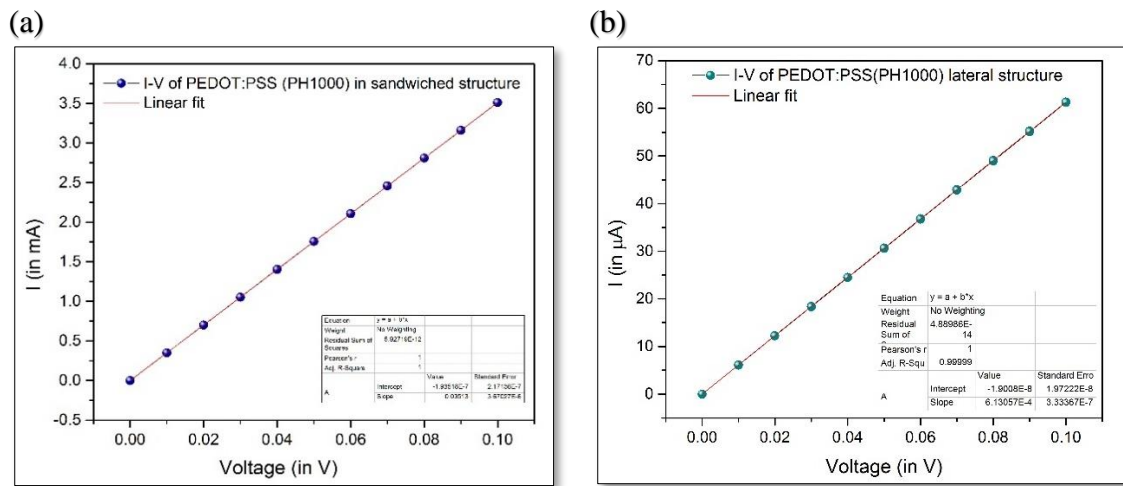


Figure (3.4) (a) Out-of plane and (b) in-plane conductivity of sandwiched and lateral structure of PEDPT:PSS (PH1000), respectively.

➤ Calculation of out-of-plane conductivity

$$\sigma = \frac{I \cdot l}{V \cdot A} = \frac{l}{R \cdot A}$$

The thickness of film, $l \sim 200\text{nm}$ (known from AFM surface roughness), Area of contact, $A \sim 2\text{mm} \cdot 2\text{mm}$. Resistance, $R \sim \frac{1}{\text{slope of } I-V} = \frac{1}{0.03513} = 28.46 \Omega$.

$$\Rightarrow \sigma_{d.c} = 1.75 \cdot 10^{-5} \text{ S/cm} \quad \dots (3.3)$$

➤ Calculation of in-plane conductivity

For the device structure used, $\frac{t}{s} = \frac{40\text{nm}}{80\mu\text{m}} \sim 10^{-4} \Rightarrow t \ll s$.

$$\rho = 4.53 \frac{V}{I} t = 4.53 \frac{1}{\text{slope of I-V}} t = 4.53 \frac{1}{6.1304E-4} t$$

$$\Rightarrow \sigma_{d.c} = 33.8 \text{ S/cm} \quad \dots (3.4)$$

The out-of plane conductivity in sandwiched structure increases only by **one-order of magnitude** for the PH1000 (the high conducting grade PEDOT:PSS) compared to the low conducting grade Al4083.

Whereas for in-plane conductivity, i.e., in lateral structure the conductivity increases by **four orders of magnitude**. Thus, only the sheet conductivity increases largely for high conducting grade (PH1000).

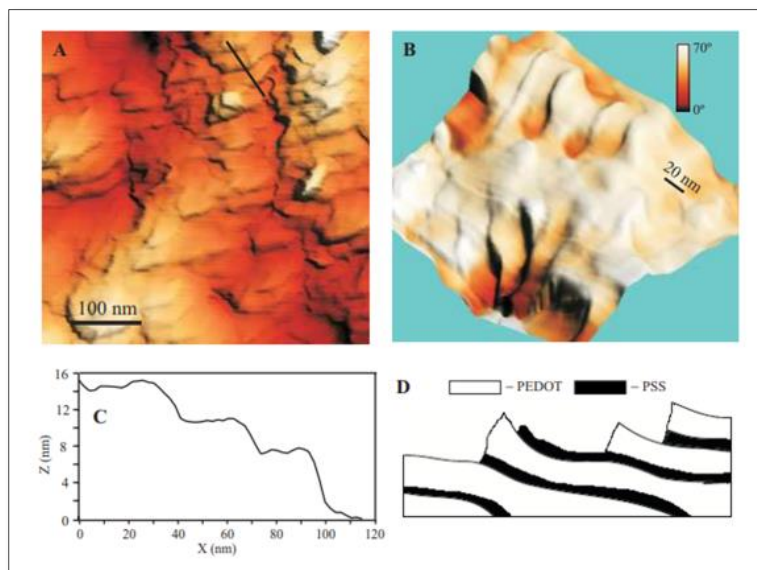


Figure (3.5): Structure of highly conducting region of PEDOT:PSS obtained from high resolution AFM scan, (B) 3D overlay of morphology and phase data at higher resolution, (C) A section profile along line segment in B. It shows the edges of several sheets, with an average step height of $\sim 3\text{nm}$. D) A schematic of the proposed PEDOT:PSS structure. (Reprinted with permission from Ref. [2] License No. 4319110870734).

It is evident from the terraced structure in figure (3.4 c) that for vertical conduction there is no continuous conduction path, i.e., the PEDOT lamellar structure (in fig 4D) is separated by PSS sheets. Thus, for vertical transport, the conduction is limited to inter-sheet barrier of PSS.

For confinement studies, narrow vertical channels are used where there is no lateral transport between the vertical barriers (insulating AAO walls). Thus, any of the two grades can be used since the vertical (out of plane) conductivity is nearly same for both grades. In the following results and discussions, I have used PEDOT:PSS A14083 grade.

(3) PEDOT:PSS + Co-solvents

Conductivity of PEDOT:PSS increases on addition of solvents like DMSO (Dimethyl sulfoxide) and E.G (Ethylene Glycol) (section 2.2.3). Different proportions of DMSO like 10wt%, 15wt%, 20wt% and 25wt% was added to PEDOT:PSS. Highest conductivity was observed for 15wt% DMSO. This matches well with the literature [3]. Similarly, for 5vol% E.G. conductivity was found to be maximum. All device structure was made to study vertical conduction, i.e., in sandwiched structure (figure 3.4).

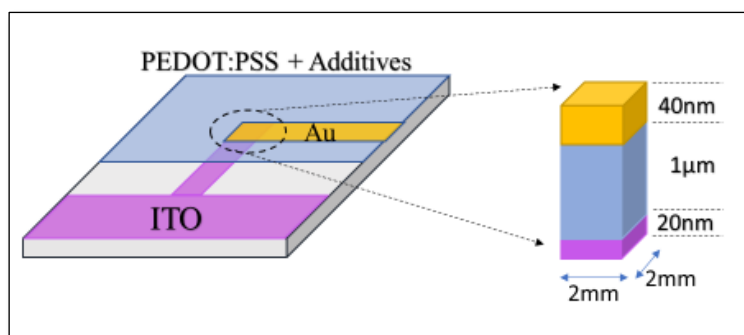


Figure (3.6): Sandwiched structure to study out-of plane conductivity of PEDOT:PSS with co-solvents. Here, the PEDOT:PSS + Additive thickness $\sim 1\mu\text{m}$.

Additives taken:

Quantity of DMSO taken = $93\mu\text{L}$ in 583.6mg PEDOT:PSS (15wt% of DMSO in PEDOT:PSS) ;

Quantity of E.G taken = 27 μ L in 583.6mg PEDOT:PSS (5vol% of E.G in PEDOT:PSS).

Four probe method has been used to measure in-plane conductivity as described earlier in section 3.1.1(1).

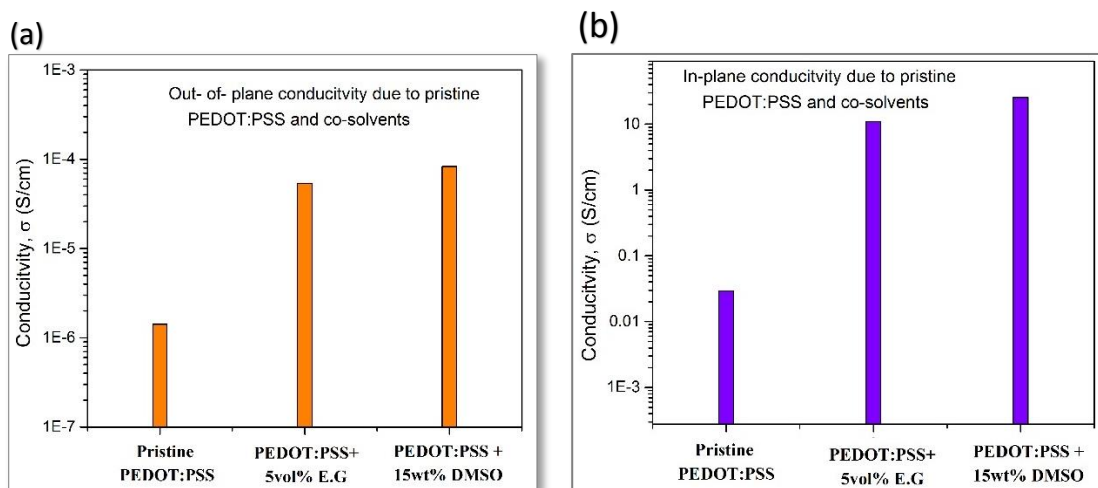


Figure (3.7): (a) out-of plane conductivity and (b) in-plane conductivity of pristine PEDOT:PSS and addition of co-solvents 5vol% E.G and 15wt% DMSO.

In-plane conductivity increases by 3 orders of magnitude on adding co-solvents. But the out-of plane conductivities increase only by nearly one order. Observed in previous reports [4].

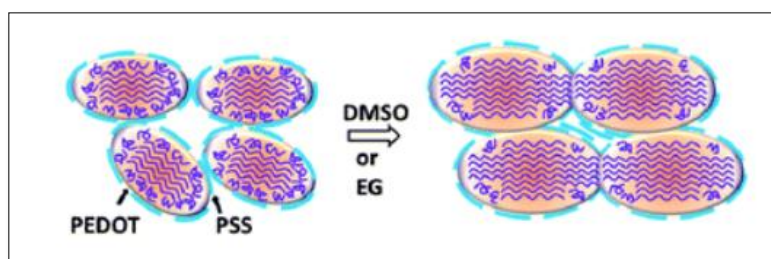


Figure (3.8): Schematic model of structural change due to addition of co-solvents (DMSO or E.G.) [5].

Addition of a co-solvent enhances the packing density of PEDOT and produces clustering among itself with reduced PSS content at the surface (as shown in figure 3.6). Besides, PSS chain network is rearranged to form closely packed domains of PEDOT nanocrystals,

which reduces defect generation at the interface [6] and results in higher device performance. The increase in the PEDOT nanocrystal size on addition of the co-solvent can be addressed to an internal re-ordering inside the nanocrystals, which is likely mediated by hydrogen bond formation between the co-solvent and PSS [7]. This co-solvent mediation stabilizes the PSS chains and realigns them along the PEDOT boundaries to allow strong packing of PEDOT crystals. Thus, the in-plane conductivity increases on addition of solvents.

➤ **Conclusion from d.c conductivity:**

The reason of low conductivity for out-of-plane of PEDOT:PSS (even on addition of co-solvents) is due to thick barriers formed by the PSS lamella that separate PEDOT-rich domains. While in lateral direction (in-plane) the PSS chains are quasi-continuous and do not form closed boundary surrounding PEDOT islands. So, conduction enhances along the PEDOT regions. The limitation of conduction caused by the inter-sheet PSS barriers during vertical transport is independent of the grade of polymer being used or added co-solvents to pristine PEDOT:PSS.

The sandwiched structured PEDOT:PSS has d.c conductivity $\sim 10^{-5}$ to 10^{-6} S/cm . The material falls under the regime of semiconductors (for values indicated below). Frequency and temperature dependent a.c conductivity will help to confirm these results.

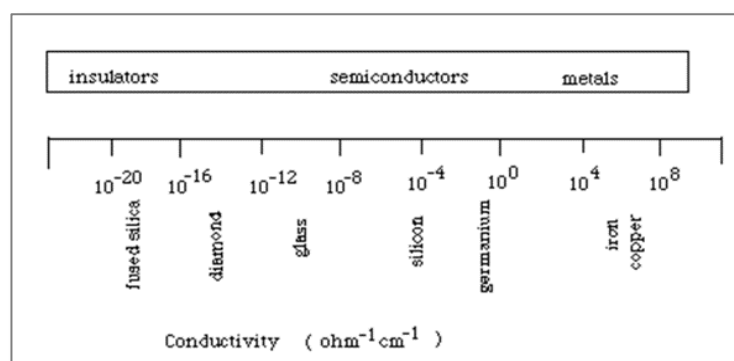


Figure (3.9) Range of electrical conductivities of metals, semiconductors and insulators.

3.1.2 Temperature dependent conductivity of pristine PEDOT:PSS

In the case of conducting polymers, conductivity is relatively high but do not behave as metals, i.e., conductivity is not increased when they are cooled. Their properties are dominated by disorder, which leads to localization of charges at low temperatures. The temperature dependence of conductivity gives information about the electrical transport mechanism.

Conductivity is measured for sandwiched structured pristine PEDOT:PSS over temperature range from 123K to 393K (using LINKAM setup mentioned in chapter2).

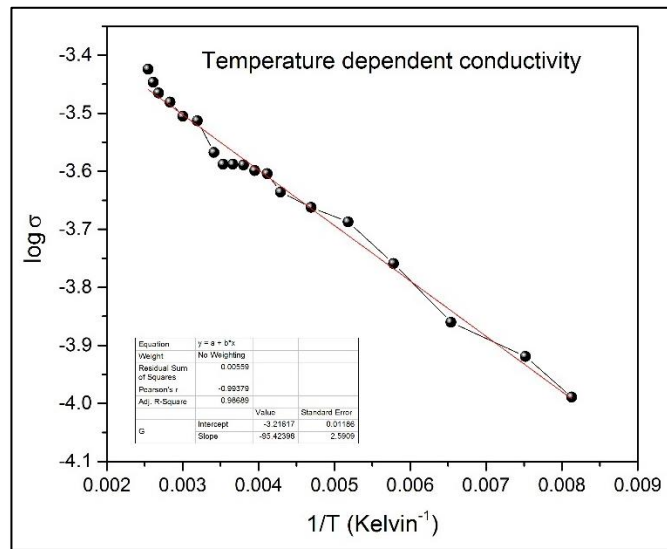


Figure (3.10) Temperature dependent conductivity for pristine PEDOT:PSS

Typically, the resulting conductivity curve can be described by: -

$$\sigma(T) = \sigma_0 \exp\left[-\left(\frac{T_0}{T}\right)^\alpha\right]$$

Here, $\alpha = 1$, which denotes nearest-neighbor hopping transport in sandwiched structure of pristine PEDOT:PSS. The reduced conductivity on lowering temperature is due to inter-sheet PSS barriers separating conducting PEDOT regions (as stated in fig 3.5).

3.1.3 A.C Conductivity

To study the frequency dependent electrical properties of the material, a.c conductivity is done. All disordered systems and semiconductors have a common feature of possessing frequency-dependent conductivity that increases approximately linearly with the increase of frequency in certain frequency regime. This universal behavior of semiconductors is given by:

$$\sigma = A \omega^s \quad (0 < s < 1) \quad \dots (3.5)$$

(where A is the pre-exponential factor dependent on temperature)

This behavior is ascribed to the relaxations caused by hopping or tunneling of charge carriers between equilibrium sites. Since in disordered material the states giving rise to the ac conductivity are clustered and do not constitute a percolation path throughout the sample (and hence do not contribute to the dc conduction), the total measured conductivity at a given frequency ω is separable into dc and ac components:

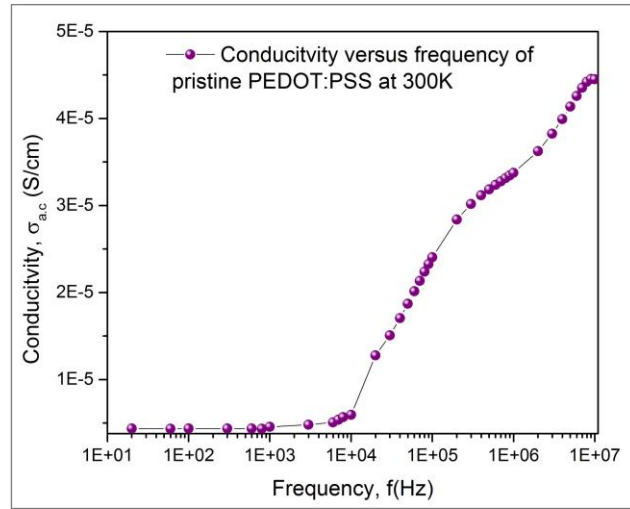
$$\sigma = \sigma_{d.c} + \sigma_{a.c}(\omega) \quad \dots (3.6)$$

Now, $\sigma_{d.c} = \sigma(\omega \rightarrow 0)$.

$$\therefore \sigma = \sigma_{d.c} + A\omega^s \quad \dots (3.7)$$

If the value of $s < 1$ then it indicates that the hopping motion is a translational one and if $s > 1$ the motion is localized one.

Here, Impedance parameters are measured for pristine PEDOT:PSS (Al4083 grade) in **sandwiched structure** (figure 3.1.b) using Semiconductor Parameter Analyzer 4200 SCS from 10kHz to 10MHz. For low frequencies (10Hz to 100kHz) lock-in amplifier SR830 is used. Electrochemical impedance is measured using a small excitation signal (small amplitude ~30 mV AC ripple on top of a controlled DC potential). This is to ensure that the system response is in linear region.



Figure(3.8): A.c conductivity of pristine PEDOT:PSS versus frequency of applied a.c signal at room temperature.

Conductivity is almost constant for frequency range from 20Hz to 10kHz ($\sigma \sim 10^{-6} \text{ S/cm} = \sigma_{d.c}$) and increases linearly with frequency till 1MHz.

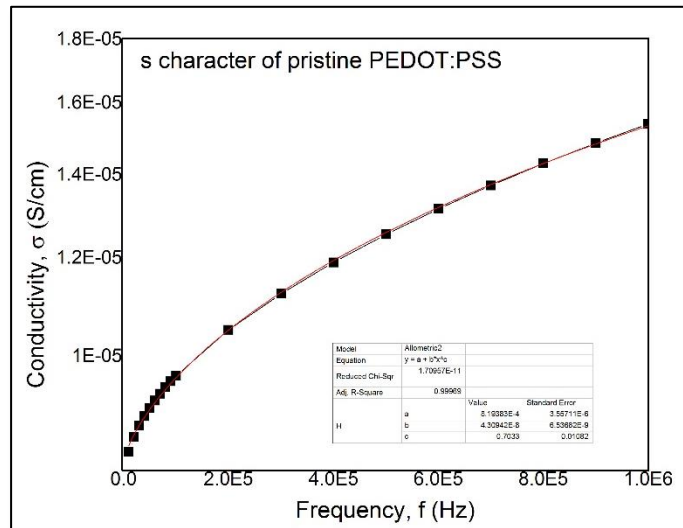


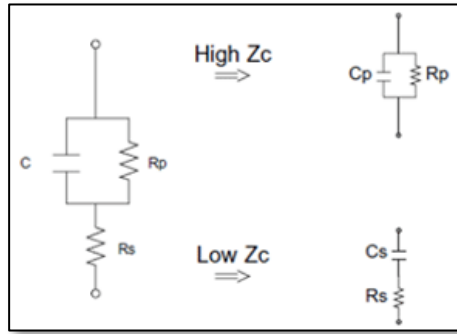
Figure (3.9): s character of pristine PEDOT:PSS at room temperature.

The conductivity versus frequency curve is fitted to eqⁿ (3.5) in frequency regime 10kHz to 1MHz. s is found to be $0.7 < 1$. So, the transport is confirmed to be hopping transport in

sandwiched structured pristine PEDOT:PSS. Hopping transport mechanism has been shown in literature reports.[^{8,9}

➤ **Calculation of conductivity from parameter analyzer:**

Parameter analyzer 4200SCS gives values for impedance Z, parallel capacitance and conductance C_p , G_p , same for series C_s and R_s . (mentioned in chapter 2).



Figure(3.10) Equivalent circuit for C_p , G_p , C_s and R_s .

Since the impedance of PEDOT:PSS along vertical direction is $> 10\text{ohms}$, so the C_p and G_p values are measured.

Parallel Capacitance, $C_p = \epsilon' \frac{A}{d}$;

Parallel Conductance, $G_p = \omega \epsilon'' \frac{A}{d} = 1/R_p$

(where permittivity $\epsilon = \sqrt{(\epsilon')^2 + \epsilon''^2}$)

$\therefore \epsilon = \frac{d}{A} \sqrt{(C_p^2 + \frac{G_p^2}{\omega^2})}$ in Farads/meter.

Dielectric constant, $k = \frac{\epsilon}{\epsilon_0}$

Conductivity, $\sigma = j\epsilon\omega = j\omega(\epsilon' - j\epsilon'')$
 $= j\epsilon'\omega + \omega\epsilon''$

$\sigma = \epsilon\omega$

This is how conductivity is calculated taking into account the area of contact between overlapping electrode and distance between them for vertical transport.

3.2 Measurements in confinement

3.2.1 D.C Conductivity

(macroscopic measurements using parameter analyzer)

Anodized Aluminum Oxide (AAO) membranes of varying pore diameter: 20 nm, 50 nm and 100 nm are used to study confinement effects on the electrical properties of PEDOT:PSS (Al4083). Sample preparation steps are mentioned in chapter 2.

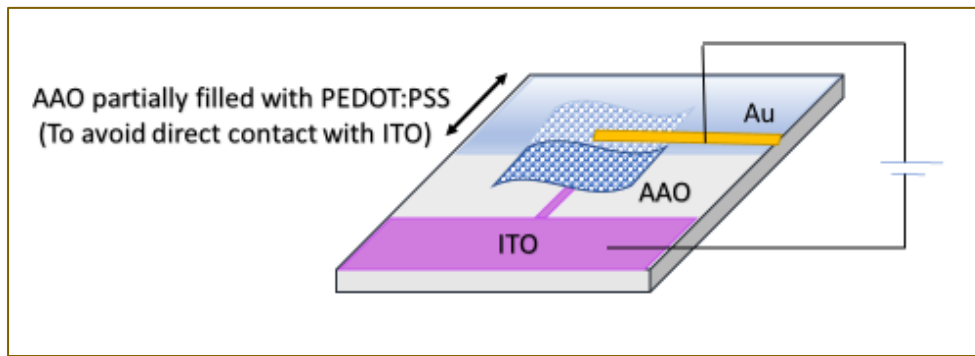


Figure (3.11) Device for studying confinement effects using two probe parameter analyzer.

This kind of device geometry is chosen to optimize conditions for the vertical transport. The polymer will have no direct contact with ITO, but only through AAO assisted vertical channels. So, the ITO has been etched out such that it finds itself well within the AAO membrane.

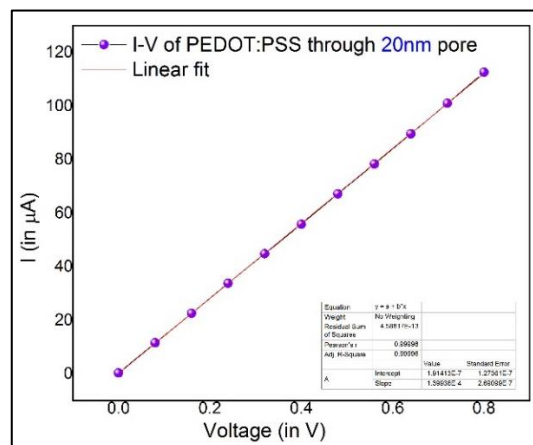


Figure (3.12): I-V characteristics of PEDOT:PSS through 20nm AAO channel

➤ **Calculation of conductivity (20nm pore):**

$$\sigma = \frac{l}{R * A_{eff}} ;$$

Where l = effective length of vertical channel filled by PEDOT:PSS

A_{eff} is the effective area of pores overlapped between ITO (bottom electrode) and Au (top electrode).

(i) **Calculation of A_{eff} :**

Let it be assumed that PEDOT:PSS fills the pore completely, $l=200\text{nm}$.

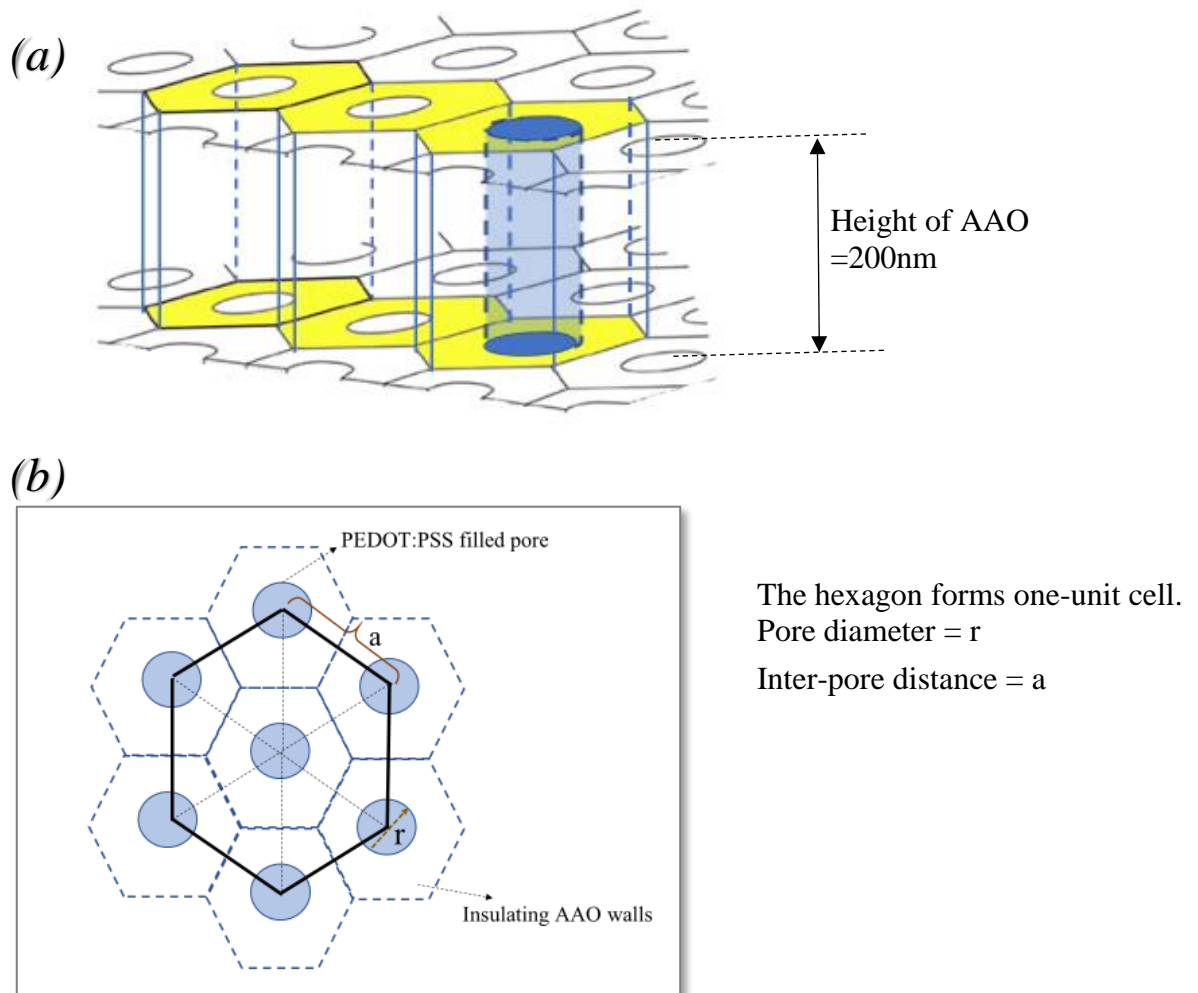


Figure (3.13)(a) Cross-sectional view and (b) top view of PEDOT:PSS filling the AAO pores.

In figure 3.13 b, the hexagon forms one unit cell containing 3 pores.

Each corner pore in the hexagon is shared by three hexagon. So, each corner pore in the hexagon contributes to $1/3^{\text{rd}}$ the total pore.

Therefore, total no. of pores in hexagon = 1 center pore + ($\frac{1}{3} * 6$ corner pores)
 $= 1 + 2 = 3$ pores

Area of circular pores (shaded blue) in the unit cell = $3 * \pi * (\frac{r}{2})^2$

Total area of unit cell (i.e., pores+walls) = $6 * \text{area of each equilateral triangles}$



Therefore, fractional overlapping area of pores = $\frac{\text{Contributing area from pores}}{\text{Total area (pores+walls)}}$
 $= \frac{3\pi(\frac{r}{2})^2}{3\frac{\sqrt{3}}{2}a^2}$

$$A_{\text{frac}} = \frac{2\pi(\frac{r}{2})^2}{\sqrt{3}a^2} = \frac{2\pi(\text{Pore radius})^2}{\sqrt{3}(\text{Inter-pore dia})^2}$$

Effective area of contact, $A_{\text{eff}} = A_{\text{frac}} * (\text{area of overlap between ITO and Au})$

In the present case for **20nm** pore diameter, interpore distance = 65nm and overlap area = $0.41 * 0.32 \text{ mm}^2$, $A_{\text{frac}} = 0.0858$;

$A_{\text{eff}} = 0.0858 * 0.41 * 0.3 \text{ mm}^2 = 0.01029 \text{ mm}^2$.

$$\sigma = \frac{l}{R * A_{\text{eff}}} = \frac{l * (\text{slope of I-V})}{A_{\text{eff}}} = 2.48 * 10^{-5} \text{ S/cm}$$

(Slope of I-V from figure 3.12)

Following the above procedure for calculation, conductivity is found for 50nm and 100nm pores also.

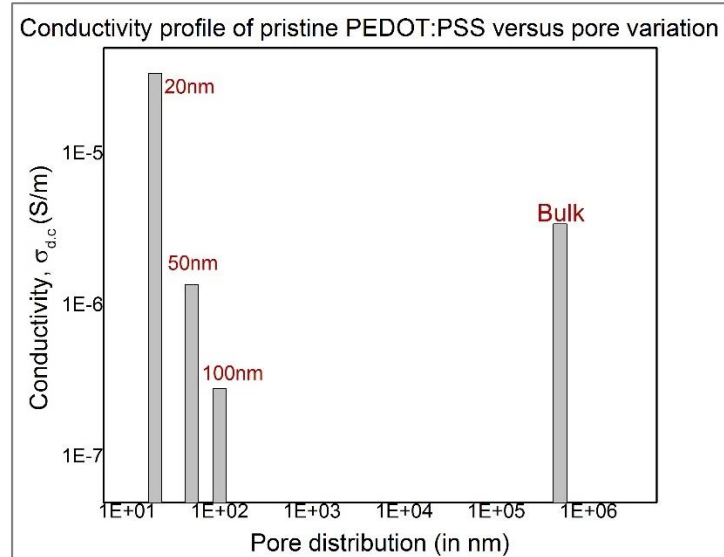


Figure (3.14) Variation of d.c conductivity of PEDOT:PSS with confinement length scales

- This calculation is done assuming the AAO pores of height 200nm are completely filled.

CAFM scans show that the pores are not completely filled and that corrections are required for the above-mentioned conductivity values.

3.2.2 D.C Conductivity using CAFM

Probing the nano-pores locally with a conducting tip (dimension~20nm) is expected to give higher accuracy of measurements over bulk measurements.

CAFM has been studied for pristine PEDOT:PSS in different AAO pore diameter.

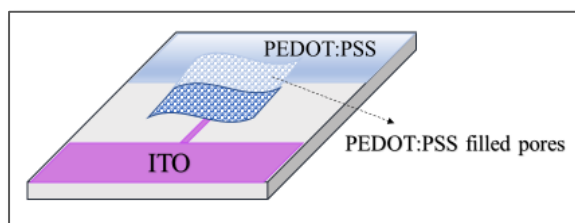


Figure (3.15): Device structure for CAFM scan

AFM and CAFM results are given below:

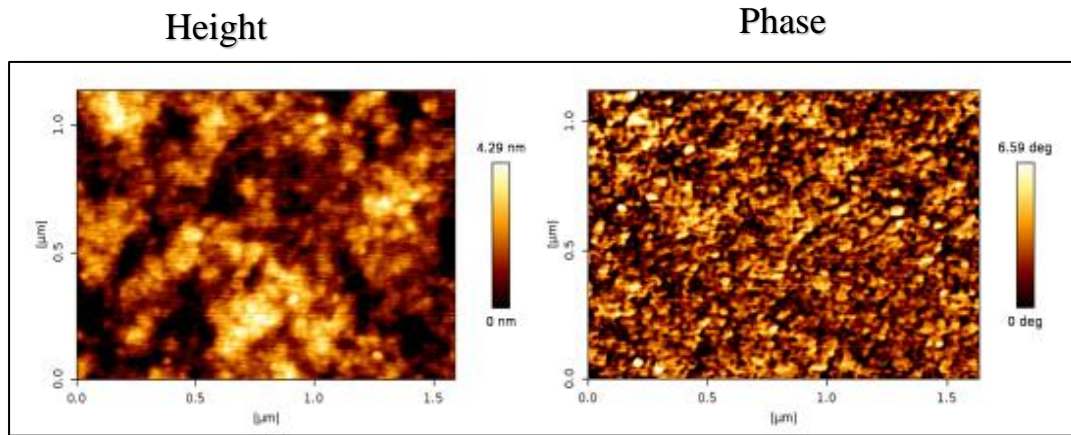


Figure (3.16) AFM surface morphology and phase of pristine PEDOT:PSS (in bulk) using non-contact mode tip.

CAFM scan showing morphology and corresponding current profile for following pore distributions:

1). Pristine PEDOT:PSS in 20nm pores

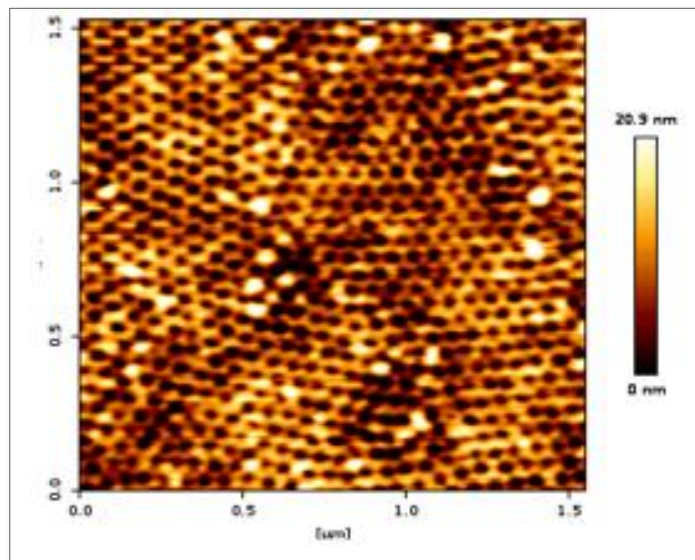


Figure (3.17): (a) Surface morphology of PEDOT:PSS filled in 20nm AAO pores

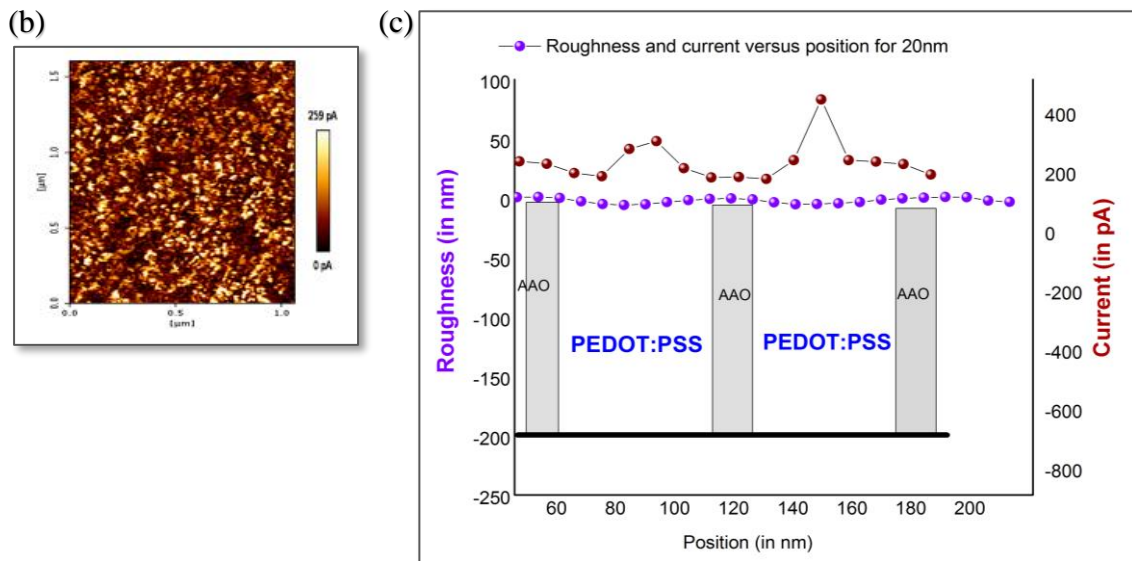


Figure (3.17): (b) Current profile of profile of PEDOT:PSS filled 20nm pores, (c) Line scan and current scan versus Graph showing the pores are almost completely filled with PEDOT:PSS (roughness of AAO surface $\sim \pm 5\text{nm}$.)

It is evident from the graph that where there are pores, i.e., the current shoots up, which is also an evidence of PEDOT:PSS filling the pores. The pores drawn in the graph shows a picture of how much length of the channel is filled by the polymer.

➤ **Calculation of conductivity in 20nm pores:**

The current values obtained in CAFM results are averaged over $> 10^4$ pores in different regions on a sample which have minimum defects (cracks originating during transfer of membranes, undulations, holes).

$$l \sim 200\text{nm}, A_{\text{eff}} \sim \pi 10^2 \text{ nm}^2, V=5\text{V}, I_{\text{avg}} = 256.74 \text{ pA}$$

$$\sigma = \frac{I_{\text{avg}} * l}{V * A_{\text{eff}}}$$

$$\sigma = 3.26 * 10^{-4} \text{ S/cm}$$

2). 50nm pores filled with pristine PEDOT:PSS

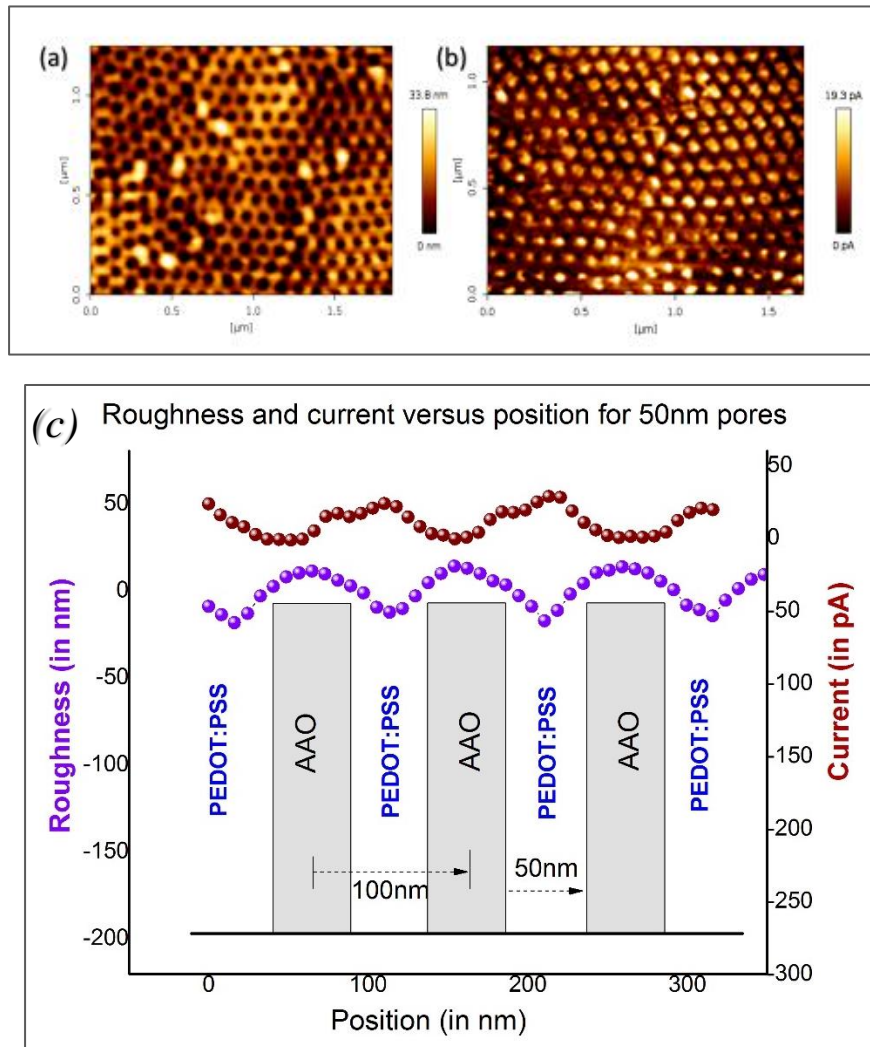


Figure (3.18): (a) Surface morphology (b) Current profile of PEDOT:PSS filled 50nm pores, (c) Line scan showing roughness (purple) and current scan marked in brown are opposite to each other, i.e., roughness shows a trough when tip enters a pore, whereas current rises due to conduction through PEDOT:PSS in pores.

The AAO Pores are drawn to scale in fig 3.18 c to give a pictorial representation of polymer filling the pore in vertical cross-section.

In this case of 50nm pores, the polymer doesn't completely fill up the pores. So, the effective column of channel contributing to current is not simply 200nm.

The effective vertical channel containing polymer contributing to current is calculated in following way:

➤ **Calculation of effective pore volume contributing to current**

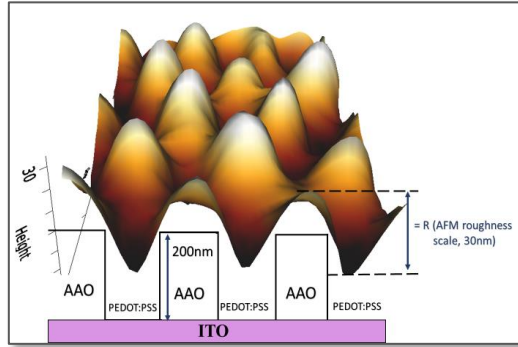


Figure (3.19): 3D image of surface morphology of 50nm pores

The image shows the vertical cross-sectional filling of polymer into the channels. As the tip traces on the surface, the tip produces the surface roughness in scan. When the cantilever tip is at position d_1 , $E=V/d_1$, V is the constant voltage applied. (figure 3.20) The vertical distance varies from d_1 , d_2 to d_3 where the current is maximum for least distance d_3 from tip to ITO electrode. (line scan and current scan as shown is figure 3.18 c).

The peak value of current is taken from the Gaussian current scan. Corresponding to the highest current in a pore gives the least distance, l =distance of tip w.r.t to ITO.

This is averaged over many pores and $I_{avg} \sim 30.54\text{pA}$

➤ **Calculation of conductivity in 50nm pores:**

$$l \sim 160.28 \pm 22.876 \text{ nm}, A_{eff} \sim \pi 25^2 \text{ nm}^2, V=5\text{v},$$

$$I_{avg} = 30.97\text{pA}$$

$$\sigma = \frac{I_{avg} * l}{V * A_{eff}}$$

$$\sigma = 5.056 * 10^{-6} (\pm 0.768 * 10^{-6}) \text{ S/cm}$$

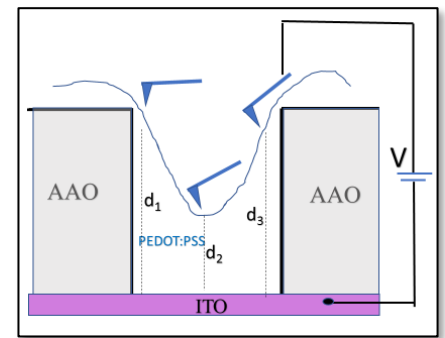


Figure (3.20) Variation of current as tip traces out partially filled pore

3). 100nm pores filled with pristine PEDOT:PSS

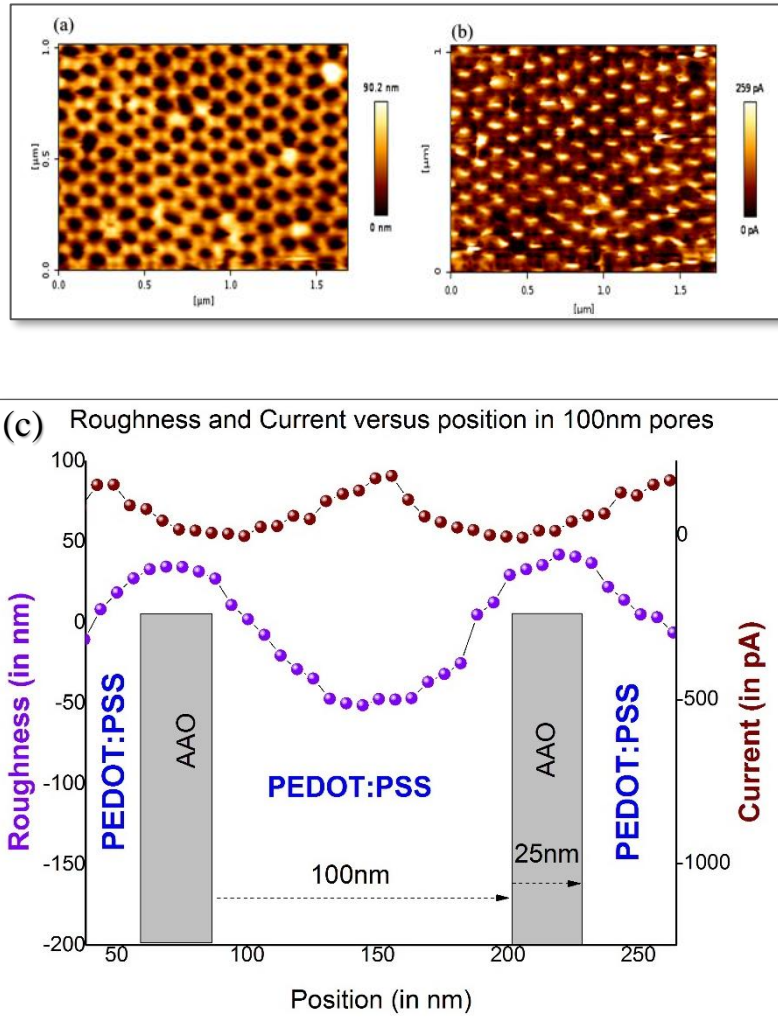


Figure (3.21): (a) Surface morphology and (b) Current profile of PEDOT:PSS filled in 100nm pores, (c) Line scan and current scan shown for the surface of 100nm pores. The schematic of AAO pores in the graph shows that the polymer filling decreases along the vertical column as pore size increases.

➤ .Calculation of conductivity in 100nm pores:

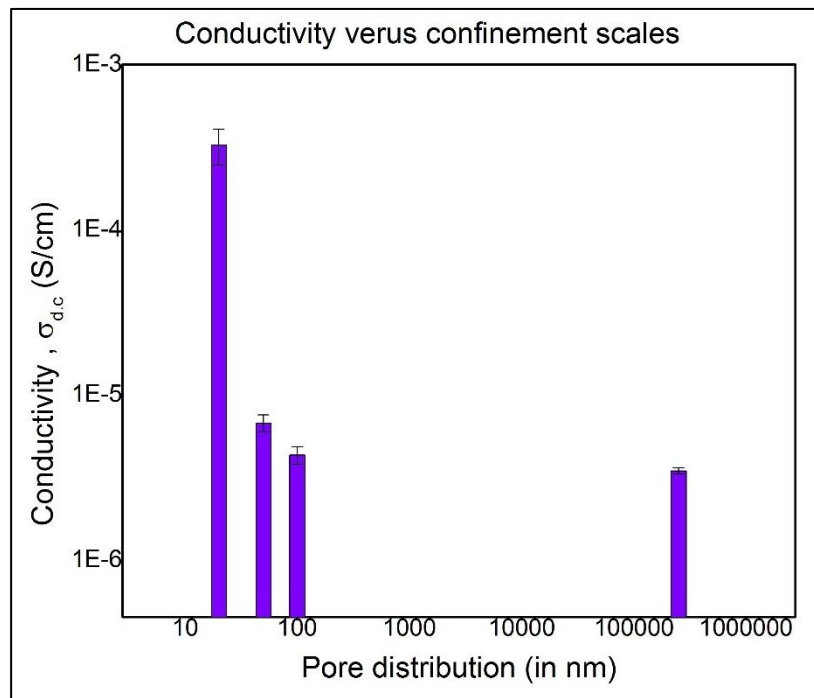
The length of polymer filling in pores, l is found from line scan. The height for all the minima in the line scan is calculated w.r.t baseline 200nm.

$$l \sim 140 \pm 18.34 \text{ nm}, A_{\text{eff}} \sim \pi 50^2 \text{ nm}^2, V=5 \text{ v}, I_{\text{avg}} \sim 120.94 \text{ pA}$$

$$\sigma = \frac{I_{avg} * l}{V * A_{eff}} ;$$

$$\sigma = 4.31 * 10^{-6} (\pm 0.523 * 10^{-6}) \text{ S/cm}$$

The error bars for conductivity in all the three above cases take into account the effective pore length contributing to current. The d.c conductivity using



Figure(3.22) Conductivity versus pore distribution using local probing of the pores (from AFM results).

➤ **Conclusion from d.c conductivity (using AFM):**

It is evident from the above results that confinement effect does play a role on conduction beyond a characteristic length scale ~20nm. If there were no confinement effects then conductivity should have decreased on reducing pore size. This is explained in figure 3.33.

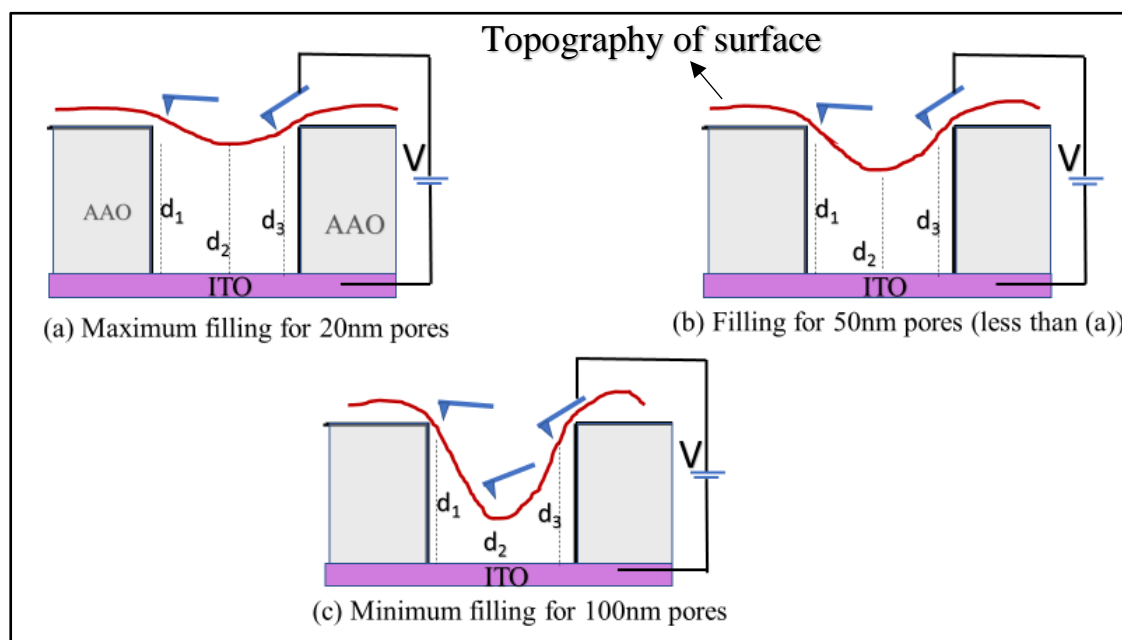


Figure (3.33) Current is measured for distance d_2 (that is the minimum distance of tip from ITO electrode which gives maximum current) inside the pores.

Comparing the pore size variation, d_2 distance is least for 100nm pores. So according to field being $E=V/d$, current should have been maximum for 100nm pore size, which is not the case. Thus, it is expected that the polymer blend PEDOT:PSS must have undergone some morphological change that increased the conductivity by two orders of magnitude on confinement (for 20nm pores).

The results obtained from macroscopic measurements using parameter analyzer gives conductivity values which are less by a factor of 3 or 4 (in case of 50nm and 100nm pores) and by an order less (for 20nm pores) than that obtained from local probing.

For macroscopic measurements, the pores were assumed to be completely filled, which is not true. Also, some other factors like cracks and defects that occur on the membranes (during transfer of membranes onto the ITO surface) can be neglected during AFM studies by probing locally uniform microscale regions, which can't be done during macroscopic studies where the ITO/polymer(in pores)/Au overlap areas $\sim \text{mm}^2$.

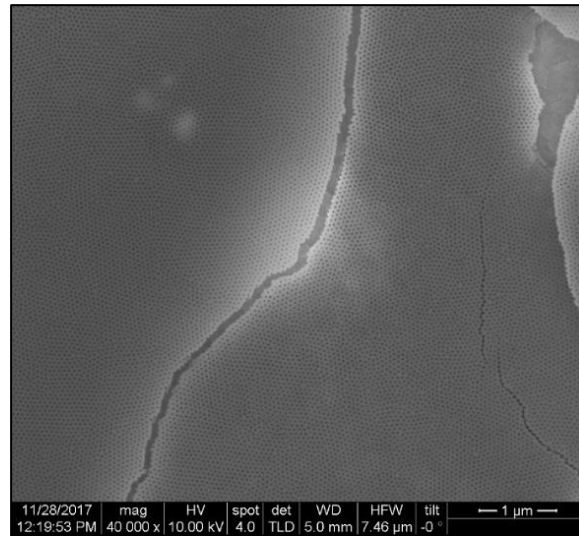


Figure (3.34): SEM image over a micrometer scales showing defects (like cracks and foldings) on the AAO membrane.

3.2.3 Temperature dependent a.c conductivity

The frequency and temperature dependence on conductivity are studied in confined channels in this section. A small A.C perturbation $\sim 30\text{mV}$ is applied to the device in figure(3.11) to study the impedance (or conductivity) of the system.

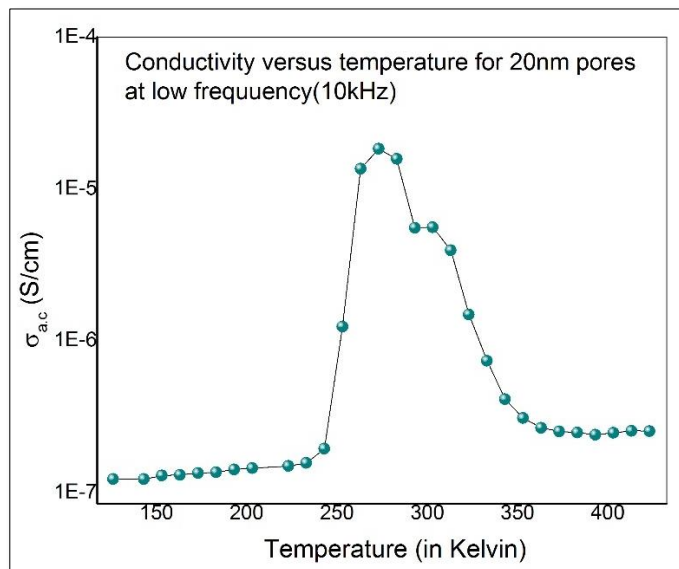
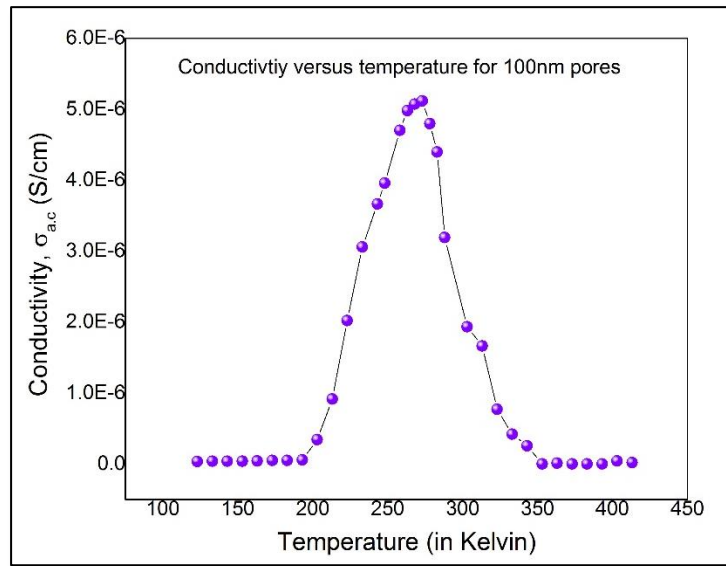


Figure (3.35) Conductivity versus temperature plot for 20nm pores.



Fig(3.36) Conductivity versus temperature plot for 100nm pores

➤ **Observations and discussions:**

- (i) The conductivity curve shows a discontinuity around 250-270K for confined channels. This doesn't occur for the pristine PEDOT:PSS film (figure 3.8). This unique behavior may be explained using eq(3.5). 's' character varies with temperature.
- (ii) At the region of discontinuity, conductivity shoots up by two orders of magnitude for 20nm pores. Whereas, for 100nm pores, the conductivity though shows discontinuity around 250K, the conductivity doesn't get magnified by orders of magnitude. It rises only by a factor of 5.

The conductivity versus frequency graph is fitted in power law $\sigma \sim \omega^s$ to get the value to s from frequency 10kHz to 1MHz. It is a temperature dependent term and plays an important role in the conduction mechanism [10].

- If s increases with temperature, a small polaron is the predominant mechanism,
- The large overlap polaron is characterized by a minimum followed by increase of s with further increase of the temperature.

- In the case where s is temperature-independent, the quantum mechanical tunneling is expected
- Correlated barrier hopping is associated with decreasing of s with the temperature.

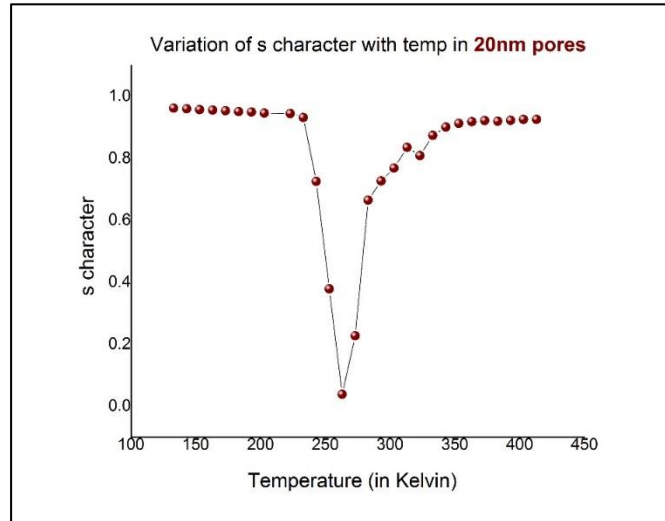


Figure (3.37): s character versus temperature for 20nm pores.

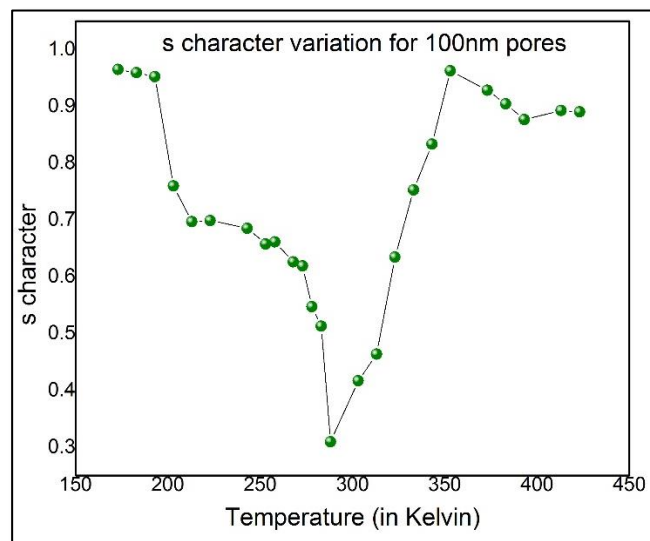


Figure (3.38): s character versus temperature for 100nm pores

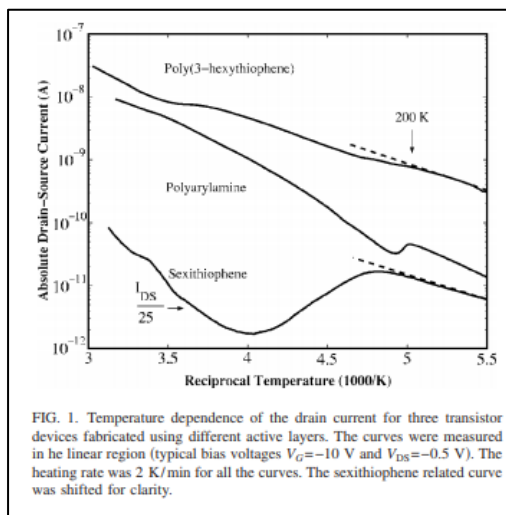
At low temperatures below 250K, hopping phenomena, i.e., correlated barrier hopping [11] takes place. At higher temperatures small polaronic effect is dominant. Further studies to low temperatures is needed to confirm if there is a semiconductor to metal

transition at all. The sudden rise in conductivity value and the supporting ‘s’ character information stating that polaron effects are small may be attributed to the rise in electronic current in 20nm pores.

But same conductivity discontinuity is observed for 100nm pores. In this case there is very small change in conductivity rise (only by a factor of 5).

In addition to the possibility that electronic current shoots up for 200nm, there may be trapping of supercooled water in the pores (which may be a reason for 100nm conductivity discontinuity).

- Confined water does not crystallize at 273 K but forms a metastable liquid. This metastable water behaves electrically as a charge trap, which causes the instability. Below 200 K the water finally solidifies and the electrical traps disappear.



Figure(3.9)[¹²] : The current decrease is caused by strong trapping, which depletes the sample from free charge carriers and is the origin of the stress effect. Below 200 K the device is stable. It is worth to mention, that the position in temperature (200 K) of the anomaly for a particular sample is independent of the heating rate and gate bias applied. Near room temperature further changes are observed in the device current, caused again by carrier trapping. These trapping effects usually start to appear above 273 K and can become clearly visible for temperatures around 280–290 K. (*Reprinted with permission from Ref[12] under Creative Commons Attribution (CC BY)*)

But changes due to trapped super-cooled water are small as shown in above ref. figure.

Further experimental support is required if truly any trace of water is trapped within the PEDOT nanocrystals. TGA analyzes shows no weight loss after heating from 140°C to 200°C.

However, the conductivity rise (by two orders of magnitude) in 20nm as compared to bulk PEDOT:PSS without pores (or other larger pores- 100nm and above) can be drawn in a schematic as follows with supporting literature reports.

3.3 Schematic of polymer blend diffusing into nanopores

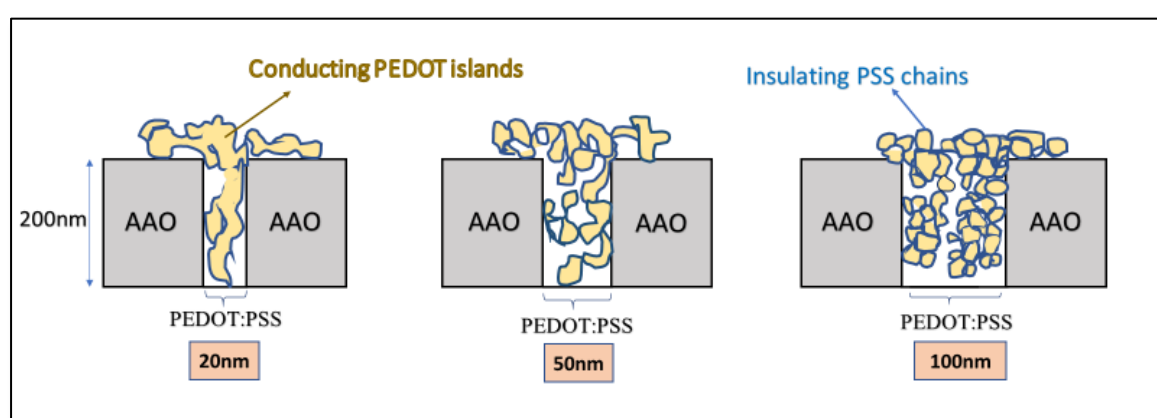
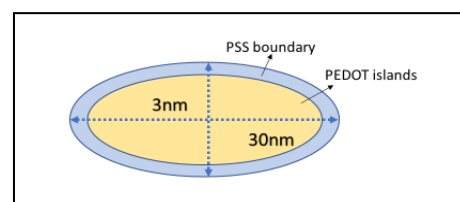


Figure (4.1) A schematic of polymer morphology change in confined channels.

Let d_{eff} be the diameter of confinement, R_{ce} = the r.m.s value of end-to-end chain length of polymer.

When degree of confinement $\delta = \frac{d_{\text{eff}}}{R_{\text{ce}}}$ is between 0.4 to 1.7, diffusion rates increase along cylindrical nanopores relative to polymer diffusion in the bulk [13].



For 100nm pores, the PSS chains form insulating barriers and hinder conduction. But as pore size decreases the diffusive transport takes place along vertical direction, assisting electronic transport over ionic at this length scale. PSS chains open up and provides path for clustering of PEDOT. Thus, for 20nm pores it may be qualitatively stated that clustering of PEDOT increases electronic conductivity to such high orders.

References:

- 1) *Ossila.com (materials science) PEDOT:PSS(AI4083) products*
- 2) C. Ionescu-Zanetti, A. Mechler, S. A. Carter, R. Lal, *Semiconductive Polymer Blends: Correlating Structure with Transport Properties at the Nanoscale, Av Material 2004, Volume 16, Issue 5*
- 3) J. Gasiorowski et al. / *Thin Solid Films 536 (2013) 211–215*
- 4) Takeya Unuma^{1,2}, Muneki Yoshikawa¹, Arao Nakamura¹ and Hideo Kishida, *Segmentation of conducting domains in PEDOT:PSS films induced by an additive for conductivity enhancement, Appl. Phys. Express 9, 051601 (2016)*
- 5) Joseph Palathinkal Thomas , *High-efficiency hybrid solar cells by nanostructural modification in PEDOT:PSS with co-solvent addition, J. Mater. Chem. A, 2014, 2, 2383-2389*
- 6) J. P. Thomas, L. Zhao, M. Abdellah, N. F. Heinig and K. T. Leung, *Anal. Chem., 2013, 85, 6840*
- 7) J. Ouyang, C. W. Chu, F. C. Chen, Q. Xu and Y. Yang, *Adv. Funct. Mater., 2005, 15, 203*
- 8) NARDES, KEMERINK, AND JANSSEN, *Anisotropic hopping conduction in spin-coated PEDOT:PSS thin films, PHYSICAL REVIEW B 76, 085208 _2007*
- 9) Cristian et al., *Semiconductor polymer blends: Correlating structure with transport properties at Nanoscale, Adv. Mat, 2004, 16,No.5*
- 10) H.M. Zaki , *Temperature dependence of dielectric properties for copper doped magnetite, Journal of Alloys and Compounds 439 (2007) 1–8*
- 11) S.R. Elliott, *A.c. conduction in amorphous chalcogenide and pnictide semiconductors, Advances in Physics, 1987, Vol. 36,No. 2,135-218*
- 12) H. L. Gomes^{a)} and P. Stallinga, *Electrical instabilities in organic semiconductors caused by trapped supercooled water, Appl. Phys. Lett. 88, 082101 (2006)*

13) Wei-Shao Tung, Russell J. Composto,^{†,‡} Robert A. Riggleman,^{*,‡} and Karen I. Winey^{*}, *Local Polymer Dynamics and Diffusion in Cylindrical Nanoconfinement*, *Macromolecules* 2015, 48, 2324–2332

CHAPTER 4

SUMMARY AND FUTURE WORK

The confinement studies on PEDOT:PSS show change in polymer blend morphology beyond a characteristic confinement length scale. The results obtained from the experimental studies done in this thesis work require additional measurements and support from simulation studies, for example, frequency dependent conduction can be studied over a broader temperature range down to 4K. Disorder effects may have pronounced role at such low temperatures that may help to understand the mechanism more specifically. Parameters (like hydrodynamic force and osmotic force balance in a capillary due to confinement) that affect the transport of carriers are to be specifically measured and studied.

However, this work opens up interesting research problems based on template structured transport. The discontinuity observed in conductivity curves if is due to trapped supercooled water then PEDOT:PSS in confined channels can act as sensors to trace amount of water.

Moving front dynamics of ions invading into a conducting polymer film is an interesting method to study ion transport in mixed ionic-electronic conducting polymers [1]. This work forms the basis of organic electrochemical transistors. This is mainly studied in planar structures. Similar things have been studied in capillaries [2]- cation invasion into an air capillary ~micron sized tube where liquid filling the air capillary is analogous to cations and holes, respectively. But the instability and non-uniformity of cation invasion front against perturbations transverse to the propagation direction, may be caused, for example, due to variation in the mixed ionic-electronic conducting film morphology. From the present study in this thesis, given the structural change of the polymer blend at characteristics length scales are known exactly then ion transport motion can be studied in a controlled way in vertical confinements at nanoscale. This will help give a relation between controlled carrier transport

on confinement against a known background of changing morphology of the transporting medium (conducting polymer) with confinement length scales. This is explained in the figure(4). Ag/AgCl electrode forms the top electrode while ITO being the bottom electrode. The top electrode is in contact with electrolyte solution on top of AAO pores. Ions are injected from electrolyte through the conducting polymer PEDOT:PSS filled AAO nano-pores.

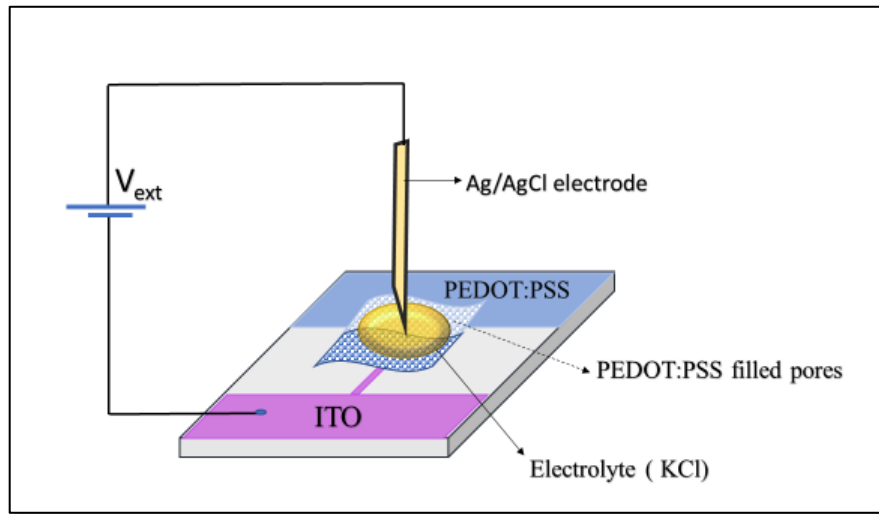


Figure (4): Schematic of proposed work- ion transport through conducting polymers in confined channels .

Any carrier conduction from electrolyte side to ITO, mediated by confined channels can be detected. The measuring parameter (may be current, impedance or conductance) of the system without the nano-channels, that is in bulk should be known prior to investigate this problem. Having a pre-knowledge of changing morphology of polymers at a characteristic confined length scale and also ion dynamics in sandwiched structure without confinement, the proposed problem may be solved.

Thereby, I conclude the thesis work with further hope to study the transport mechanisms with more controlled parameters in confinement which may confirm these findings.

References:

- 1) Stavrinidou E, Leleux P, Rajaona H, Khodagholy D, Rivnay J, Lindau M, Sanaur S, Malliaras GG. Direct measurement of ion mobility in a conducting polymer., *Adv Mater.* 2013;25:4488–4493.
 - 2 Saffman PG, Taylor G. The penetration of a fluid into a porous medium or Hele–Shaw cell containing a more viscous liquid. *Proc R Soc London A Math Phys Sci.*1958;245(1242):312–329.
-